Paxillin inhibits HDAC6 to regulate microtubule acetylation, Golgi structure, and polarized migration

Nicholas O. Deakin and Christopher E. Turner

Department of Cell and Developmental Biology, State University of New York Upstate Medical University, Syracuse, NY 13210

Polarized cell migration is essential for normal organism development and is also a critical component of cancer cell invasion and disease progression. Directional cell motility requires the coordination of dynamic cell–extracellular matrix interactions as well as repositioning of the Golgi apparatus, both of which can be controlled by the microtubule (MT) cytoskeleton. In this paper, we have identified a new and conserved role for the focal adhesion scaffold protein paxillin in regulating the posttranslational modification of the MT cytoskeleton through an inhibitory interaction with the α-tubulin deacetylase HDAC6. We also determined that through HDAC6-dependent regulation of the MT cytoskeleton, paxillin regulates both Golgi organelle integrity and polarized cell invasion and migration in both three-dimensional and two-dimensional matrix microenvironments. Importantly, these data reveal a fundamental role for paxillin in coordinating MT acetylation-dependent cell polarization and migration in both normal and transformed cells.

Introduction

Cell polarization and subsequent directional migration are of fundamental importance to a variety of essential physiological processes including embryogenesis, tissue repair, and immune surveillance (Ridley et al., 2003). The migration machinery is also used in a variety of diseases, such as metastatic cancer in which enhanced cell motility and invasion is concomitant with poor prognosis and decreased patient survival (Gupta and Massagué, 2006; Steeg, 2006). A prerequisite for polarized cell motility is the establishment of a distinct cell front and rear, characterized in migratory cells by a leading edge of membrane protrusion and a retracting tail. Indeed, for productive, directional cell migration, both propulsive traction forces at the front and retraction of the rear must be tightly coupled (Ridley et al., 2003). In the vast majority of migratory cells, the adhesive forces are generated by integrin-mediated structures known as focal adhesions (FAs) or adhesion contacts, which form a physical link between the cell and its surrounding ECM-rich microenvironment.

Paxillin is a key component of the cellular adhesome (Zaidel-Bar et al., 2007) in which it primarily functions as a molecular scaffold to spatiotemporally integrate diverse signaling networks to transduce and coordinate dynamic, intracellular responses to a variety of stimuli (Brown and Turner, 2004; Deakin and Turner, 2008). For example, through its interactome, paxillin has been shown to regulate FA growth, stabilization, and disassembly to enable migration on 2D surfaces (Webb et al., 2004) as well as invasion through 3D-ECM (Deakin and Turner, 2011), possibly through Rho GTPase-driven changes in its molecular interactions with proteins such as vinculin and actopaxin (α-parvin; Deakin et al., 2012).

A further key element of cell polarization is the directed trafficking of newly synthesized, promigratory factors to the appropriate cellular locale (Bergmann et al., 1983; Schmoranzer et al., 2003), such as the accumulation of active Cdc42 and its effector β-PIX at the leading edge (Osmani et al., 2010) as well as α5 integrin to the cell rear to enable directionally persistent migration (Theisen et al., 2012). In the majority of motile cells examined on 2D ECM, polarized trafficking is achieved by reorganization and posttranslational modification of the microtubule (MT) cytoskeleton as well as through reorientation of a cohesive Golgi apparatus to a position ahead of the nucleus in the direction of migration (Bisel et al., 2008; Miller et al., 2009). The juxtanuclear positioning of the Golgi apparatus is regulated by the MT cytoskeleton. Indeed, in the absence of MTs, the Golgi

Correspondence to Christopher E. Turner: turnerce@upstate.edu

Abbreviations used in this paper: apFRET, acceptor photobleaching FRET; CDM, cell-derived matrix; co-IP, coimmunoprecipitation; FA, focal adhesion; FRET, fluorescence resonance energy transfer; HDAC, histone deacetylase; HFF, human foreskin fibroblast; MEF, mouse embryonic fibroblast; MFI, mean fluorescence intensity; MT, microtubule; PLA, proximity ligation assay; SIRT2, sirtuin-2.

The Rockefeller University Press $30.00
J. Cell Biol. Vol. 206 No. 3 395–413
www.jcb.org/cgi/doi/10.1083/jcb.201403039

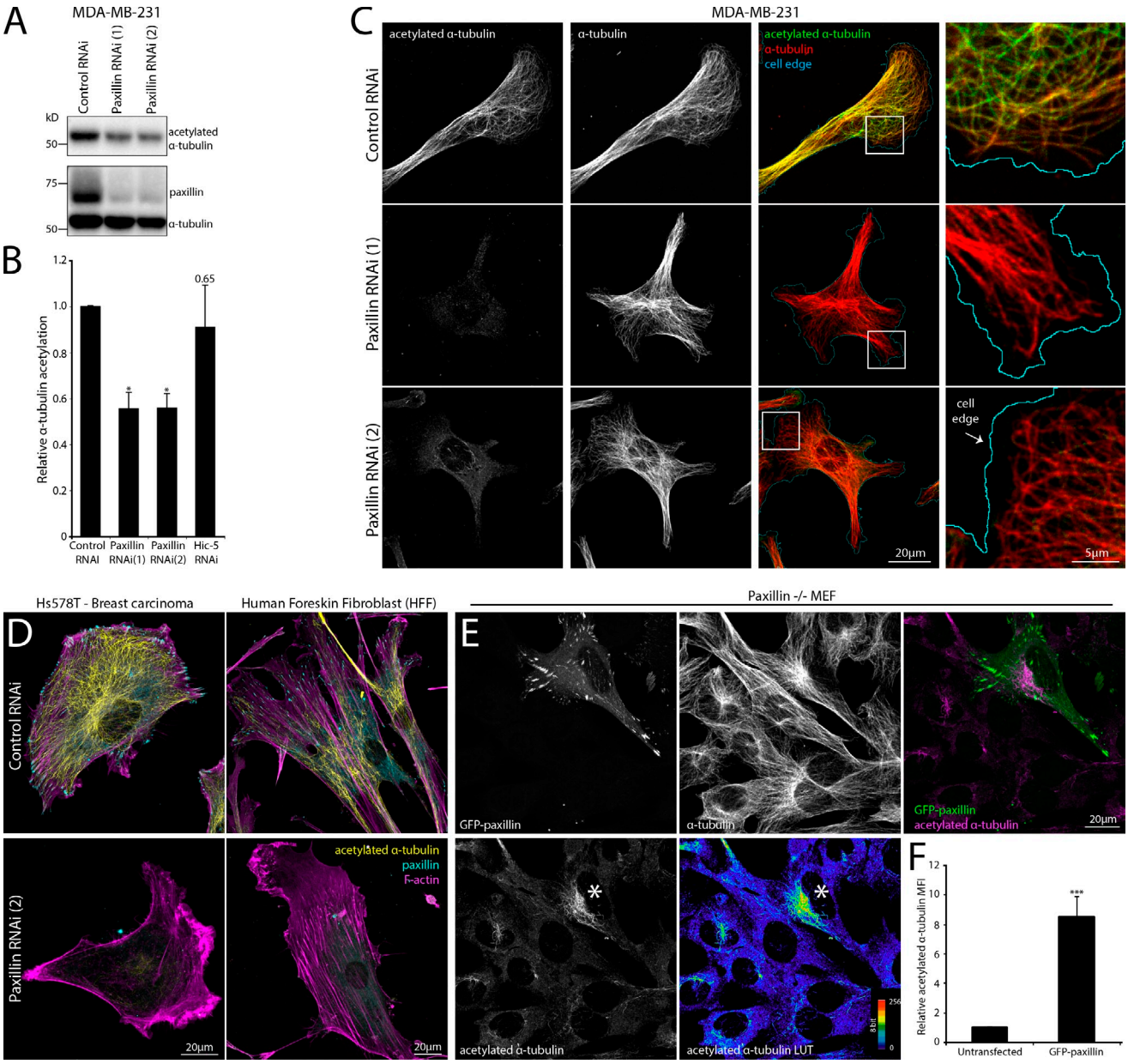

Figure 1. **Paxillin regulates MT acetylation in malignant and normal cell types.** (A–C) Western blot (A) quantitation (B), and images (C), indicating a reduction in α-tubulin acetylation upon paxillin depletion in MDA-MB-231 cells. Boxed regions indicate the area of the merged image used for the zoom. RNAi-mediated Hic-5 protein depletion did not significantly affect α-tubulin acetylation ($P = 0.65$). $n = 3$ individual experiments. (D) Images of microtubule (MT) acetylation in Hs578T and HFF cells after paxillin depletion. (E and F) Images (E) and quantitation (F) of mean fluorescence intensity (MFI) of acetylated α-tubulin immunofluorescence in paxillin$^{-/-}$ MEFs reexpressing GFP-paxillin, as indicated by the asterisks. Pseudocolored lookup table (LUT) images highlight changes in acetylated α-tubulin pixel MFI. $n = 3$ individual experiments, and MFI from a minimum of 21 cells was quantified. Data are represented as the mean ± SEM. *, $P < 0.05$; ***, $P < 0.0005$.

fragments and the constituent ministacks disperse, resulting in perturbation of polarized secretion and migration (Skoufias et al., 1990; Rodionov et al., 1993; Thyberg and Moskalewski, 1999). Furthermore, repeated stable MT targeting to FAs accompanies their disassembly (Ezratty et al., 2005), highlighting cooperation between these complex structures. Hence, the stability of the MT network is essential for cell polarization and directional migration.

It is widely accepted that acetylation of α-tubulin at lysine 40 is a posttranslational modification that is associated with more stable, long-lived, and less dynamic MTs (Maruta et al., 1986; Cambray-Deakin and Burgoyne, 1987; Piperno et al., 1987; Houliston and Maro, 1989; Webster and Borisy, 1989; Thyberg and Moskalewski, 1993; Matsuyama et al., 2002; Tran et al., 2007; Matov et al., 2010). Furthermore, acetylated MTs are significantly enriched at the Golgi apparatus and have been implicated in establishing a cohesive organelle (Thyberg and Moskalewski, 1993; Burkhardt, 1998; Ryan et al., 2012). Importantly, acetylated MTs have been shown to exhibit a polarized enrichment toward the leading edge during directional 3D migration (Doyle et al., 2009) and in response to 2D cell monolayer wounding (Yadav et al., 2009). Acetylation of α-tubulin also

enhances kinesin-1–mediated anterograde trafficking (Reed et al., 2006), indicating that this modification likely serves an active role in promoting cell polarization as opposed to merely being a marker of MT longevity or stability.

Acetylation of MTs in mammalian cells is positively regulated by a variety of acetyltransferases, including, but not limited to, α-TAT1 (α-tubulin *N*-acetyltransferase 1) and the Elongator protein complex (Creppe et al., 2009; Akella et al., 2010). To date, the histone deacetylase (HDAC) family member HDAC6 and sirtuin-2 (SIRT2) are the only described α-tubulin deacetylases (Hubbert et al., 2002; North et al., 2003). HDAC6 is unique among the HDAC family, as it contains two functional deacetylase domains (Valenzuela-Fernández et al., 2008) and exhibits direct interactions with a variety of diverse proteins, including dynein and the protein phosphatase PP1 (Kawaguchi et al., 2003; Chen et al., 2005). Moreover, HDAC6 has been shown to be upregulated in numerous cancers, in which it has been linked to increased cell invasion and metastasis (Inoue et al., 2002; Sakuma et al., 2006; Rey et al., 2011; Kanno et al., 2012; Zuo et al., 2012). The mechanisms of HDAC6 activation have been extensively studied and include phosphorylation by aurora A, PKC-α, GRK2, and GSK3-β (Pugacheva et al., 2007; Chen et al., 2010; Zhu et al., 2011; Lafarga et al., 2012). In contrast, the proteins responsible for the inhibition of HDAC6 in both normal and malignant cells remain elusive but are of paramount importance for the development of effective targeted therapeutics for the potential efficacious treatment of cancers (Aldana-Masangkay and Sakamoto, 2011). Herein, we identify an entirely new and ubiquitous role for paxillin as a regulator of cell polarization and directional motility through its ability to regulate MT acetylation and Golgi structural integrity through its interaction with and inhibition of HDAC6.

Results

Paxillin regulates MT acetylation through inhibition of the α-tubulin deacetylase HDAC6

It has previously been shown that paxillin is capable of influencing the dynamics of MTs at FAs through an as-yet-undetermined mechanism (Efimov et al., 2008). Moreover, paxillin is also necessary for coupling front protrusion and rear retraction during 3D invasive migration (Deakin and Turner, 2011) as well as localized activation of Cdc42 (Deakin et al., 2009) and accumulation of key polarity proteins (Yu et al., 2009) at the leading edge of migrating cells. Importantly, each of these aforementioned processes can be regulated by dynamic changes in the MT cytoskeleton, through maintaining and repositioning an integral Golgi apparatus (Nagasaki and Gundersen, 1996; de Forges et al., 2012). Therefore, we sought to determine whether paxillin is able to regulate the cell polarization and migration machinery through influencing the organization and/or function of the MT cytoskeleton.

Despite the previously described interaction between paxillin and α-tubulin (Brown and Turner, 2002), we observed no gross disruption in the architecture of the MT cytoskeleton in either malignant cells or fibroblasts lacking paxillin expression (Fig. 1, A, C, and E). However, RNAi-mediated depletion of paxillin in the highly invasive MDA-MB-231 breast adenocarcinoma cell line resulted in a significant decrease in α-tubulin acetylation at lysine 40 (Fig. 1, A and B). In contrast to paxillin-depleted cells, RNAi of Hic-5, a closely related paxillin family member, had no effect on the global levels of acetylated α-tubulin (Fig. 1 B). Importantly, depletion of paxillin in other malignant (Hs578T breast carcinoma) and normal (human foreskin fibroblast [HFF] and NIH-3T3) cell types also resulted in a reduction of α-tubulin acetylation (Fig. 1 D; Fig. S1, A and D; and not depicted). Furthermore, paxillin-null mouse embryonic fibroblasts (MEFs) also exhibited a lack of MT acetylation, which could be rescued by reexpression of GFP-tagged paxillin (Fig. 1, E and F). Collectively, these data identify a novel and fundamentally conserved role for paxillin in the regulation of MT acetylation in both transformed and normal cells.

The acetylation of polymerized α-tubulin at Lys40 is tightly controlled by the enzymatic activity of multiple acetyltransferases and negatively regulated through the activity of deacetylases HDAC6 (Hubbert et al., 2002) and to a lesser extent, SIRT2 (North et al., 2003). Therefore, we hypothesized that paxillin may be acting to promote MT acetylation through either enhancing the activation of acetyltransferases or through inhibition of the predominant tubulin deacetylase. Consistent with previous results (Haggarty et al., 2003; Tran et al., 2007; Zuo et al., 2012), suppression of HDAC6 activity by the specific inhibitor tubacin resulted in an enhancement of MT acetylation in control RNAi-treated MDA-MB-231 cells. A similar result was observed after RNAi of HDAC6 (Fig. 2 A and Fig. S2). Either pharmacologic inhibition of HDAC6 or RNAi-mediated HDAC6 depletion was able to efficiently rescue α-tubulin acetylation in cells lacking paxillin (Fig. 2 A), suggesting that cells lacking paxillin likely have enhanced HDAC6 activation rather than dysfunctional acetyltransferases. In addition, no significant change in HDAC6 protein expression was observed after paxillin RNAi (Fig. 2, A and F). In contrast to a previous study (North et al., 2003), but consistent with studies using fibroblasts and tissues isolated from SIRT2-null mice (Zhang et al., 2008; Bobrowska et al., 2012) RNAi-mediated depletion of SIRT2, the only other identified MT deacetylase, had no significant effect on α-tubulin acetylation at Lys40 (Fig. 2 B). Similarly, MT acetylation was also rescued in paxillin-depleted HFF and Hs578T cells upon treatment with tubacin or after HDAC6 depletion using RNAi (Fig. S1, A and D). These data therefore identify HDAC6 as the predominant α-tubulin deacetylase and demonstrate an important role for paxillin in the regulation of its activity.

The fundamental mechanisms of HDAC6 inactivation, in either malignant or normal cells, have yet to be determined. To assess HDAC6 activity regulated by paxillin, cells were treated with tubacin for 16 h to ensure maximal MT acetylation (Fig. 2, C and E). Subsequently, the inhibitor was removed, and the rate of α-tubulin deacetylation was assessed both biochemically and through immunofluorescence microscopy. The initial rate of deacetylation of α-tubulin in paxillin-depleted cells was significantly enhanced relative to control cells (Fig. 2 D), with maximal α-tubulin deacetylation being achieved after 120 min (Fig. 2, C and E). Importantly, no gross defect in the MT cytoskeleton was observed. However, it is worth noting that analysis of the

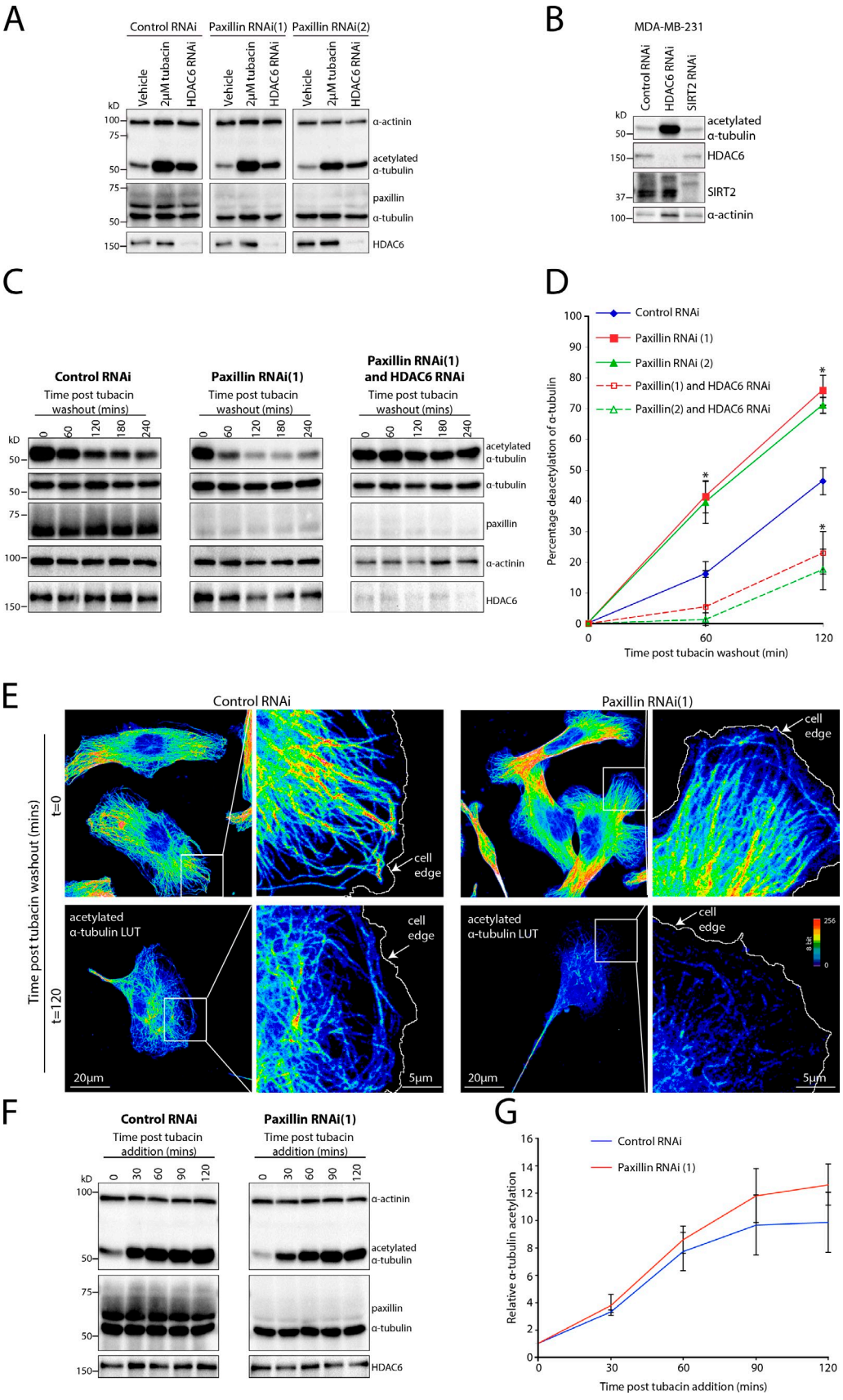

Figure 2. **Paxillin depletion promotes MT deacetylation through activation of HDAC6.** (A) Western blots of MDA-MB-231 cells treated with control or paxillin RNAi as indicated, with 2 μM tubacin for 4 h or HDAC6 RNAi. (B) RNAi of SIRT2, another α-tubulin deacetylase, had minimal effect on global α-tubulin acetylation as assessed by Western blot analysis. (C–E) Western blots (C), quantitation (D), and images (E) of α-tubulin deacetylation after

immunofluorescence images after tubacin washout indicated that, in control cells, deacetylation of MTs appeared to be initially restricted to the leading edge of cell protrusion (Fig. 2 E). In contrast, the acetylated α-tubulin staining was robustly lost throughout the paxillin-depleted cells early after tubacin removal (Fig. 2 E and not depicted). To confirm the requirement for HDAC6 in paxillin-mediated MT deacetylation, paxillin-depleted cells were also treated with HDAC6 RNAi, which significantly attenuated the deacetylation observed in cells lacking paxillin alone (Fig. 2, C and D). We suspect that the small decrease in α-tubulin deacetylation observed in cells lacking paxillin and HDAC6 after tubacin washout (Fig. 2, C and D) is most likely caused by incomplete HDAC6 knockdown (Fig. 2 C), which was determined to be routinely >85%. Importantly, no significant difference in acetyltransferase activity was observed between control and paxillin RNAi-treated cells, as determined by measuring the rate of α-tubulin acetylation upon HDAC6 inhibition with tubacin (Fig. 2, F and G).

Paxillin interacts with HDAC6 in normal and transformed cells

Paxillin functions primarily as a protein scaffold (Brown and Turner, 2004; Deakin and Turner, 2008). Therefore, we hypothesized that it may be inhibiting HDAC6 activity through a molecular interaction. A possible association between the two endogenous proteins was initially examined using an in situ proximity ligation assay (PLA). Consistent with an interaction between paxillin and HDAC6, numerous PLA-positive spots were observed throughout both MDA-MB-231 (Fig. 3, A and B) and HFF cells (not depicted) that were not observed using control antibodies (Fig. 3, A and B). A robust association between endogenous paxillin and HDAC6 was also confirmed by coimmunoprecipitation (co-IP; Fig. 3, C and D).

Paxillin is enriched in integrin-mediated FAs but is also membrane associated and cytosolic (Deakin and Turner, 2008; Deakin et al., 2012), whereas HDAC6 appears diffuse and generally cytosolic (Hubbert et al., 2002). To further examine the subcellular localization of the paxillin and HDAC6 interaction, we used acceptor photobleaching fluorescence resonance energy transfer (FRET; apFRET). This is a technique we have previously used to spatiotemporally resolve paxillin interactions with both vinculin and actopaxin (Deakin et al., 2012). Consistent with previous studies (Valenzuela-Fernández et al., 2005; Liu et al., 2012), GFP-tagged HDAC6 was predominantly cytosolic (Fig. 3 E). Interestingly, the apFRET analyses indicated a close proximity between the two proteins throughout the cell but also some localized enrichment of the complex coincident with and juxtaposed to large FAs (Fig. 3, E–G). To further assess the existence of paxillin–HDAC6 complexes at FAs, we repeated the PLA analyses using MDA-MB-231 cells in which adhesion structures were demarcated through the expression of GFP-tagged talin. Quantitative image analysis revealed that, consistent with the apFRET (Fig. 3 E), a small fraction of the observed PLA spots were indeed at least partially colocalized with talin-GFP–positive adhesion structures (Fig. 3 H, insets). For comparison, analysis of paxillin's interaction with FAK, using the same approach, indicated that almost 60% of the paxillin-FAK PLA spots colocalized with talin-GFP (Fig. 3 H). Costes' randomization method for measurement of colocalization (Costes et al., 2004) was used to confirm, with >95% certainty, that the colocalization observed between the paxillin and HDAC6 PLA spots and FAs was not caused by chance coincidence. Collectively with the FRET analysis, these data suggest that paxillin interacts with HDAC6 predominantly in the cytosol to suppress its activity and control global MT acetylation, whereas the presence of a small population of paxillin–HDAC6 complexes at or around FAs may be more important for regulating localized MT function.

The proline-rich region of paxillin is required for the association with HDAC6 to regulate MT acetylation

Paxillin has a well-defined domain structure, with the majority of its interactions mediated by its N-terminal LD motifs, in particular LD1, LD2, and LD4 (Fig. 4 A; Brown and Turner, 2004). Rather surprisingly, as with GFP-paxillin, expression of GFP-paxillin mutants lacking either the LD1, LD2, or LD4 motifs rescued MT acetylation in paxillin-null MEFs (Fig. 4 B and not depicted). However, despite targeting efficiently to FAs, a GFP-paxillin mutant lacking the proline-rich region (GFP-paxillinΔPro) was unable to significantly increase MT acetylation above levels observed in GFP-expressing or neighboring untransfected controls (Fig. 4, B and C). This lack of rescue indicates that the proline-rich region is required to promote MT acetylation. Furthermore, both co-IP (Fig. 4 D) and PLA analyses (Fig. 4, E and F) demonstrate that the proline-rich region of paxillin is essential for its association with HDAC6.

Paxillin regulates HDAC6-mediated MT acetylation to control directional invasive migration

We have previously identified paxillin as a critical component of the migration machinery in both 2D and 3D microenvironments, in which it serves to control adhesion dynamics and phenotypic plasticity to modulate breast cancer cell invasion and metastasis (Deakin and Turner, 2011). HDAC6 activity and its concomitant effects on MT acetylation levels have also been shown to influence adhesion stability, invasion, and directional cell motility (Hubbert et al., 2002; Cabrero et al., 2006; Tran et al., 2007; Zhang et al., 2007). Therefore, we sought to determine whether the elevated HDAC6 activity observed in paxillin-depleted cells contributed to the inability of MDA-MB-231 cells to exhibit polarized 3D migration/invasion. As previously reported for this cell type, paxillin RNAi significantly inhibited cell invasion into a 3D collagen and fibronectin-rich ECM

tubacin washout. Boxed regions indicate the area used for the respective zoomed images. LUT, lookup table. (F and G) Western blots (F) and quantitation (G) of the time course of α-tubulin acetylation after the addition of 2 µM tubacin. Data are represented as the mean ± SEM. *, $P < 0.05$ from $n = 3$ individual experiments.

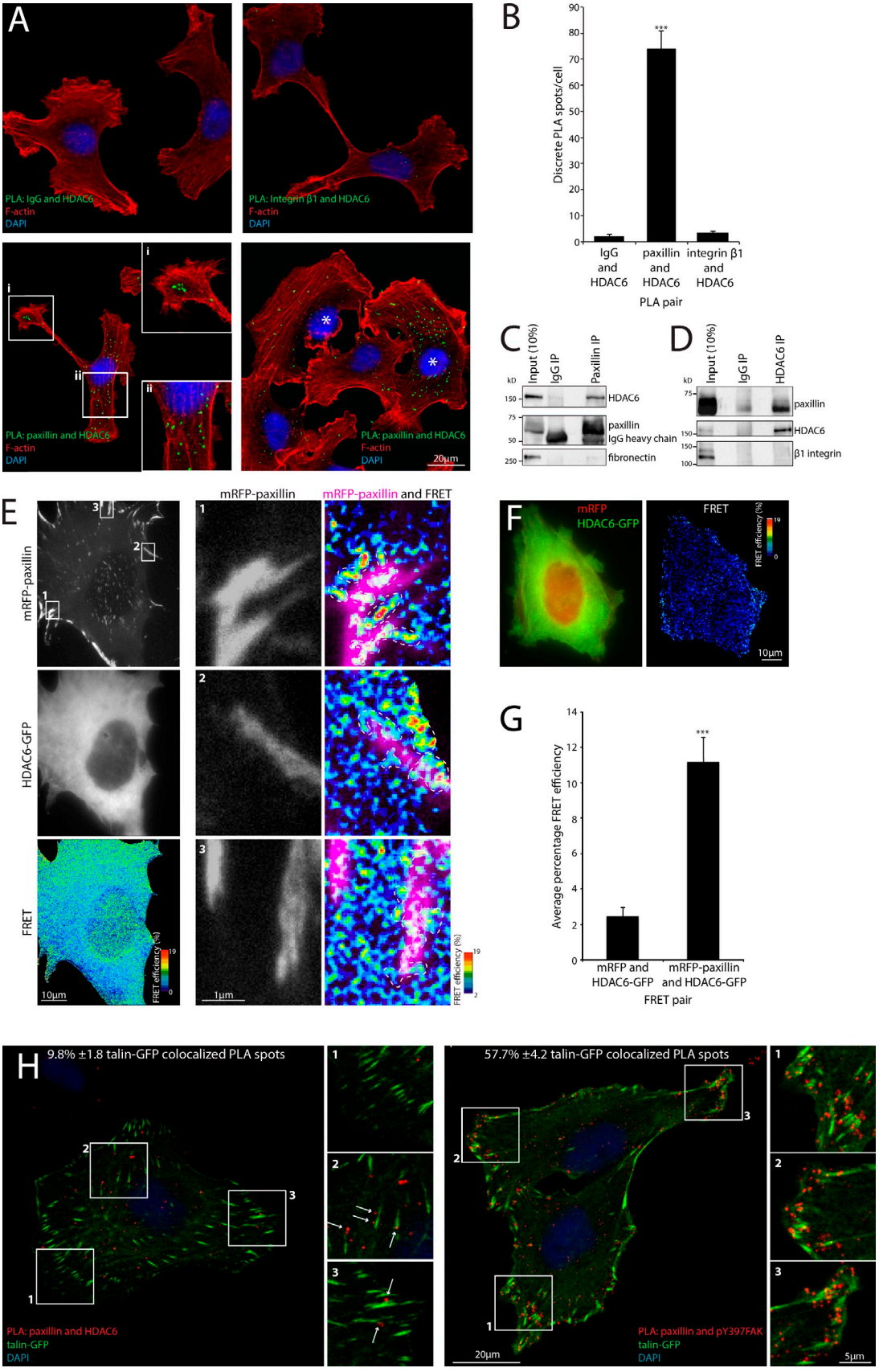

Figure 3. **Endogenous paxillin and HDAC6 exhibit a direct interaction throughout the cell.** (A and B) Representative images (A) and quantitation (B) of a proximity ligation assay (PLA) performed in MDA-MB-231 cells with protein-specific antibody pairs as indicated. Asterisks highlight cells with the most PLA spots and robust F-actin stress fibers. (C and D) Western blots of endogenous paxillin co-IP with HDAC6 in MDA-MB-231 cells. (E and F) Images of paxillin$^{-/-}$

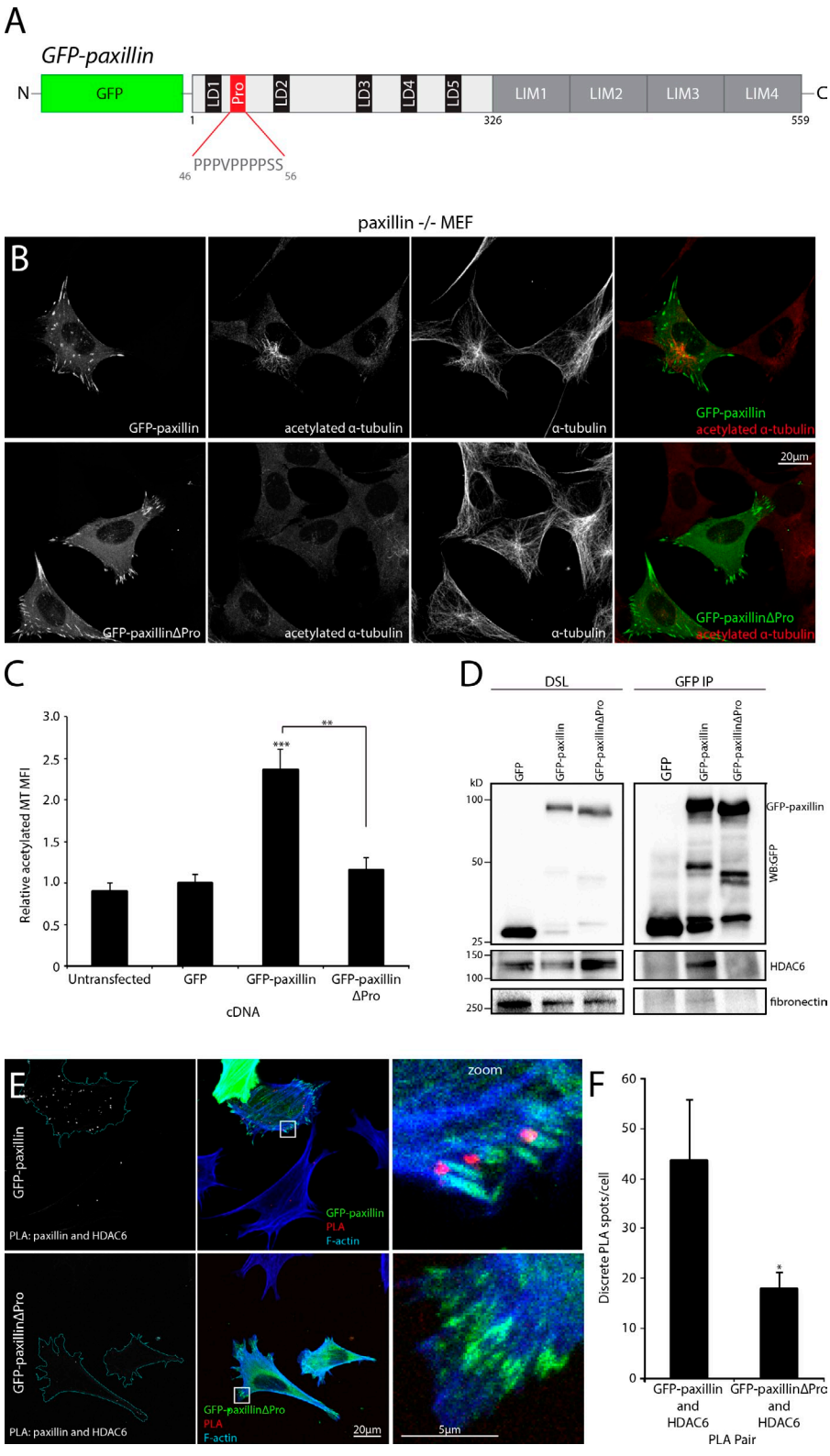

Figure 4. **Paxillin regulates HDAC6 activity through its proline-rich region.** (A) Schematic representation of the domain structure of paxillin. The proline-rich region (Pro) is demarcated in red and spans amino acids 46–56, which are deleted in the GFP-paxillinΔPro construct. N, N terminus; C, C terminus. (B and C) Images of paxillin$^{-/-}$ MEFs transfected with GFP-tagged paxillin constructs as indicated. Cells were plated on fibronectin-coated coverslips 16 h before fixation, immunofluorescence staining, and relative acetylated α-tubulin MFI quantitation (C). MFI was quantified from a minimum of 17 cells from three individual experiments. (D) Western blots of GFP-paxillin co-IP with endogenous HDAC6 in paxillin$^{-/-}$ MEFs. WB, Western blot. Equal protein input was determined by Western blotting of the respective detergent soluble lysates (DSL). (E and F) Images (E) and quantitation (F) of PLA spots between the GFP-tagged paxillin constructs as indicated and endogenous HDAC6. Boxed regions indicate the area used for the respective zoomed images. Data are represented as the mean ± SEM. *, P < 0.05; **, P < 0.005; ***, P < 0.0005.

MEFs expressing mRFP-paxillin and HDAC6-GFP (E) or mRFP and HDAC6-GFP (F) subjected to apFRET. Dashed lines demarcate hot spots of FRET associated with FAs. (G) Quantitation of the FRET efficiency between FRET pairs as indicated. FRET values were quantified from a minimum of 16 cells and three individual repeats. (H) Images of MDA-MB-231 cells expressing GFP-tagged talin and analyzed using a PLA as indicated. PLA spot colocalization with talin-GFP (arrows) was determined from a minimum of 13 cells from $n = 2$ individual experiments. Data are represented as the mean ± SEMs. ***, P < 0.0005. Boxed regions indicate the areas used for the zoomed insets and cropped images.

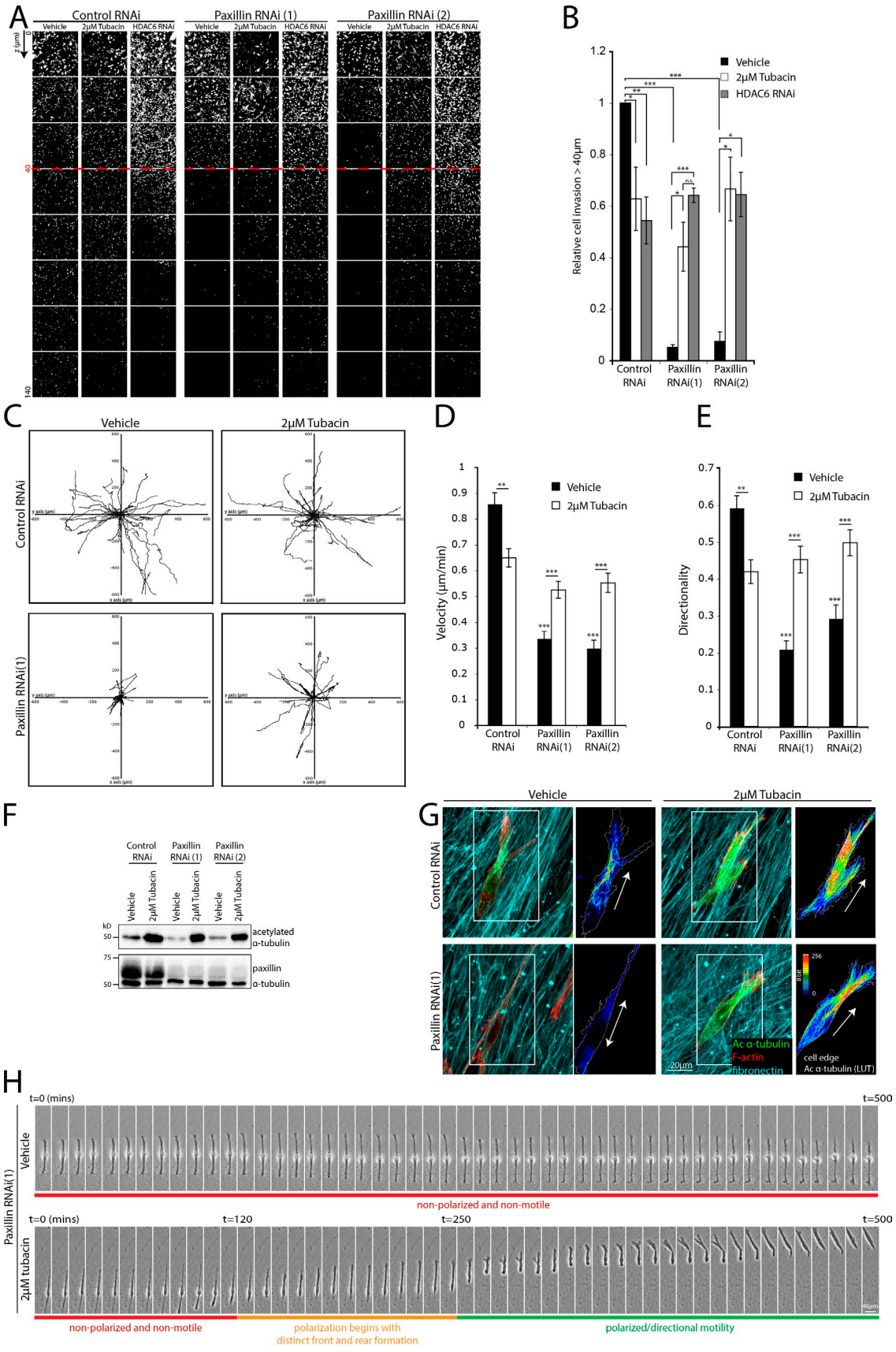

Figure 5. **Inhibition of HDAC6 activity rescues invasion, 3D motility, polarized MT acetylation, and cell morphology in paxillin-depleted cells.** (A and B) Montages (A) and quantitation (B) of MDA-MB-231 cell invasion into collagen- and fibronectin-rich 3D gels. *n* = 4 individual experiments. (C–E) Migration tracks (C), velocity (D), and directionality analysis (E) of MDA-MB-231 cell migration through 3D CDMs. A minimum of 30 tracks from three individual

(Fig. 5, A and B). Furthermore, consistent with work by others in fibroblasts and cancer cell lines (Tran et al., 2007; Zhang et al., 2007), HDAC6 inhibition by treatment with tubacin or HDAC6 depletion, using RNAi, significantly perturbed cell invasion (Fig. 5, A and B). Interestingly, HDAC6 inhibition or ablation in cells lacking paxillin resulted in a significant rescue of cell invasion (Fig. 5, A and B). These data suggest that the increase in HDAC6 activity and associated hypoacetylation of MTs in paxillin-depleted cells is, at least in part, responsible for the decrease in their invasive capacity. Importantly, the rescue was comparable to the level of invasion observed in control RNAi-treated cells lacking HDAC6 activity (Fig. 5 B), indicating that optimal 3D motility likely requires tight regulation of both MT acetylation and deacetylation.

To visualize changes in polarized 3D migration, we performed motility analyses in cell-derived matrices (CDMs). The matrix organization observed in these CDMs (Cukierman et al., 2001; Deakin and Turner, 2011) is reminiscent of the ECM architecture at the tumor–stroma boundary in vivo, where parallel fibrous ECM protein arrays have been observed (Provenzano et al., 2006). As a result of the aligned ECM fibers characteristic of HFF-derived CDMs, control RNAi-treated MDA-MB-231 cells use a persistent, polarized mode of motility (Fig. 5, C, E, and G). In contrast, cells lacking paxillin adopt an elongated nonmotile phenotype (Fig. 5, G and H) with a significant reduction in both cell migration velocity and directionality (Fig. 5, D and E) as previously described (Deakin and Turner, 2011). Similarly, pharmacologic inhibition of HDAC6 in control RNAi cells significantly decreased both migration velocity and directionality (Fig. 5, C–E). In contrast, HDAC6 inhibition with tubacin in cells lacking paxillin resulted in a significant rescue in MT acetylation (Fig. 5, F and G) as well as polarized cell motility (Fig. 5, C–E), consistent with the increase in 3D invasion (Fig. 5, A and B). Comparable results to the tubacin-mediated rescue of migration in cells lacking paxillin were also obtained when cells were treated with both paxillin and HDAC6 RNAi (unpublished data).

Consistent with a previous study of fibroblasts migrating through 3D CDMs (Doyle et al., 2009), there was a robust enrichment of acetylated MTs directed toward the leading edge in control RNAi-treated cells (Fig. 5 G). In contrast, paxillin-depleted cells exhibited a nonpolarized morphology with no distinct front or rear as well as a significant decrease in MT acetylation (Fig. 5, F and G). Importantly, suppression of HDAC6 activity by addition of tubacin as well as RNAi-mediated HDAC6 depletion resulted in an increase in polarized MT acetylation in both control and paxillin RNAi-treated cells (Fig. 5, F and G; and not depicted). Furthermore, cells lacking paxillin expression also reestablished a polarized morphology shortly after tubacin addition with the formation of a distinct cell front and rear, before commencing directional migration (Fig. 5 H). This effect was not restricted to invasive MDA-MB-231 cells or 3D migration because polarized 2D cell motility, as determined using a wound-healing assay, was also rescued in paxillin-depleted Hs578T cells and HFFs treated with tubacin or HDAC6 RNAi (Fig. S1). Collectively, these data identify paxillin as a key modulator of HDAC6 activity in the regulation of polarized migration in both 3D and 2D microenvironments.

Paxillin is required for MT acetylation-mediated Golgi cohesion and positioning in 2D and 3D ECM

A fundamental requirement in the establishment of polarization in mammalian cells during cell migration is the repositioning of the condensed Golgi apparatus ahead of the nucleus as well as the directed stabilization of the MT cytoskeleton. A polarized Golgi is thought to be necessary for targeting the trafficking of pro-migratory factors to the leading edge (Nagasaki and Gundersen, 1996; de Forges et al., 2012; Stehbens and Wittmann, 2012). The intimate relationship between the Golgi apparatus and the MT cytoskeleton has been well documented in 2D systems. Indeed, it has been suggested that acetylated MTs are enriched at and required for establishment of the Golgi as a cohesive interconnected organelle (Thyberg and Moskalewski, 1993). In accordance with these previous observations, control RNAi-treated MDA-MB-231 cells plated on a 2D substrate exhibited an enrichment of acetylated MTs toward the apparent direction of motility and also at the Golgi apparatus (Fig. 6 A). Furthermore, the Golgi was characteristically compact (Fig. 6 A). In contrast, paxillin depletion with RNAi resulted in an overt fragmentation of the Golgi apparatus in >80% of cells, with numerous disparate giantin-positive Golgi objects observed (Fig. 6, A and B). Quantitation of the fragmentation phenotype confirmed a significant increase in the number of discrete, smaller Golgi objects in cells lacking paxillin (Fig. 6, C and D). Furthermore, analysis of Golgi morphology in paxillin-depleted Hs578T cells and HFFs also revealed striking fragmentation (Fig. S3), consistent with a fundamental role for paxillin in maintaining MT acetylation-dependent Golgi integrity. It is unlikely that the increase in Golgi objects was caused by a change in Golgi protein expression as no significant increase in giantin (Fig. 6 E) or GM130 (see Fig. 9 A) levels was seen in the paxillin-depleted cells.

To assess the link between paxillin and Golgi cohesion in an inherently polarized system, cells were placed in 3D CDMs, and Golgi morphology as well as associated cell phenotype and MT acetylation were examined. Similar to 2D systems, paxillin-depleted cells exhibited a highly disorganized, fragmented Golgi apparatus, a lack of MT acetylation and a nonpolarized morphology (Fig. 6, F and G). Importantly, treatment with tubacin (Fig. 6 F) or HDAC6 RNAi (Fig. S4) resulted in a rescue of Golgi compaction in paxillin-depleted cells, as demonstrated by a significant reduction in the number of discrete Golgi objects (Fig. 6 G) and an increase in average Golgi object area (Fig. 6 H).

experiments was used for 3D migration analyses. (F and G) Western blots (F) and images (G) showing a rescue of α-tubulin acetylation in cells treated with paxillin RNAi and 2 µM tubacin during 4 h of 3D migration. Arrows indicate direction of migration, and boxed regions indicate the cropped region used for the pseudocolored acetylated (Ac) α-tubulin lookup table (LUT) image. (H) Representative kymographs from 3D CDM migration time-lapse videos of paxillin-depleted MDA-MB-231 cells treated with vehicle or 2 µM tubacin at $t = 0$. Data are represented as the mean ± SEM. *, $P < 0.05$; **, $P < 0.005$; ***, $P < 0.0005$.

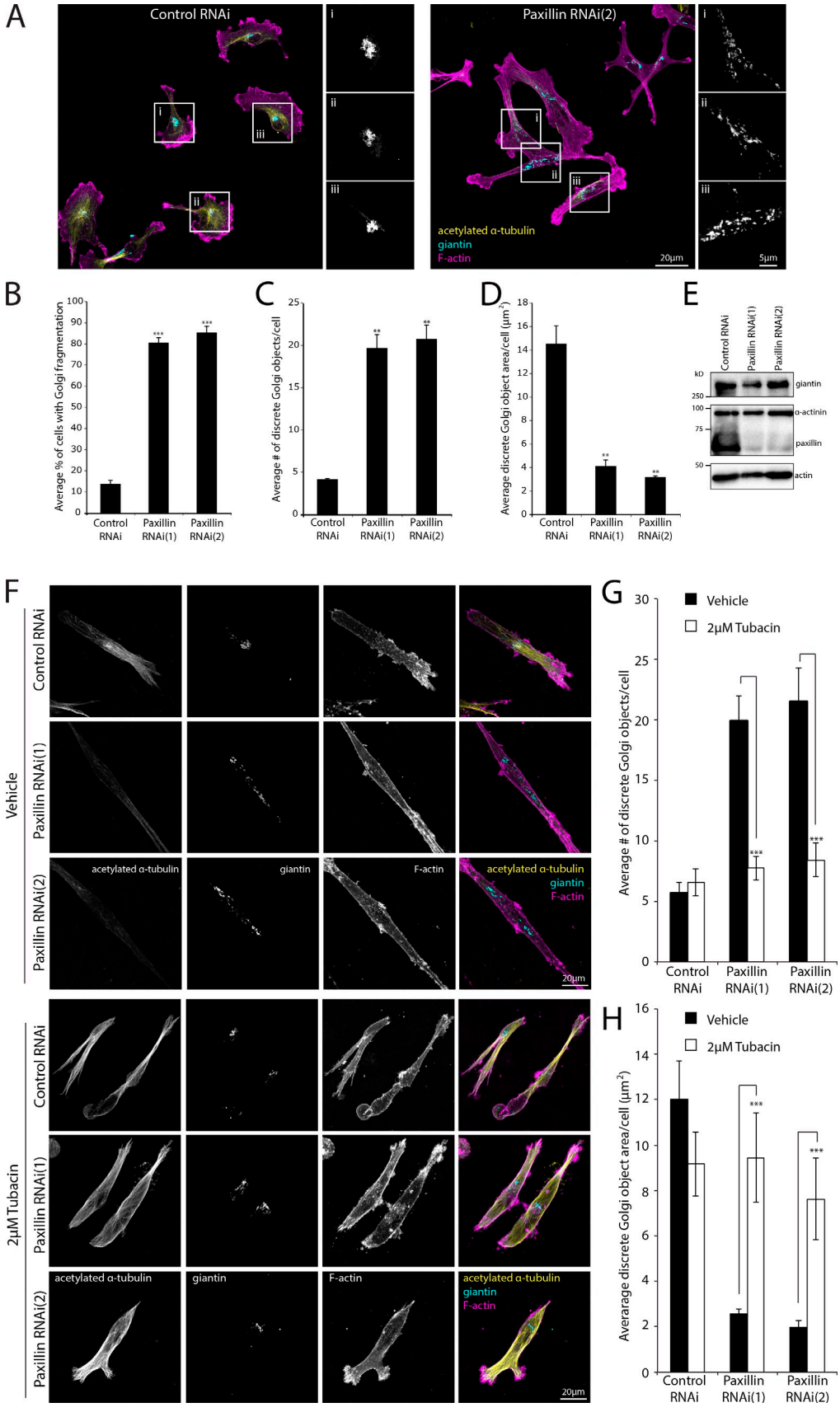

Figure 6. **Paxillin depletion in MDA-MB-231 cells promotes Golgi fragmentation in 2D and 3D microenvironments, which can be rescued by HDAC6 inhibition.** (A) Images of the Golgi fragmentation phenotype observed in MDA-MB-231 cells lacking paxillin. Boxed regions indicate the area used for the respective zoomed giantin images. (B–D) Quantitation of the percentage of RNAi-treated cells with a fragmented Golgi (B) and the number (C) and average

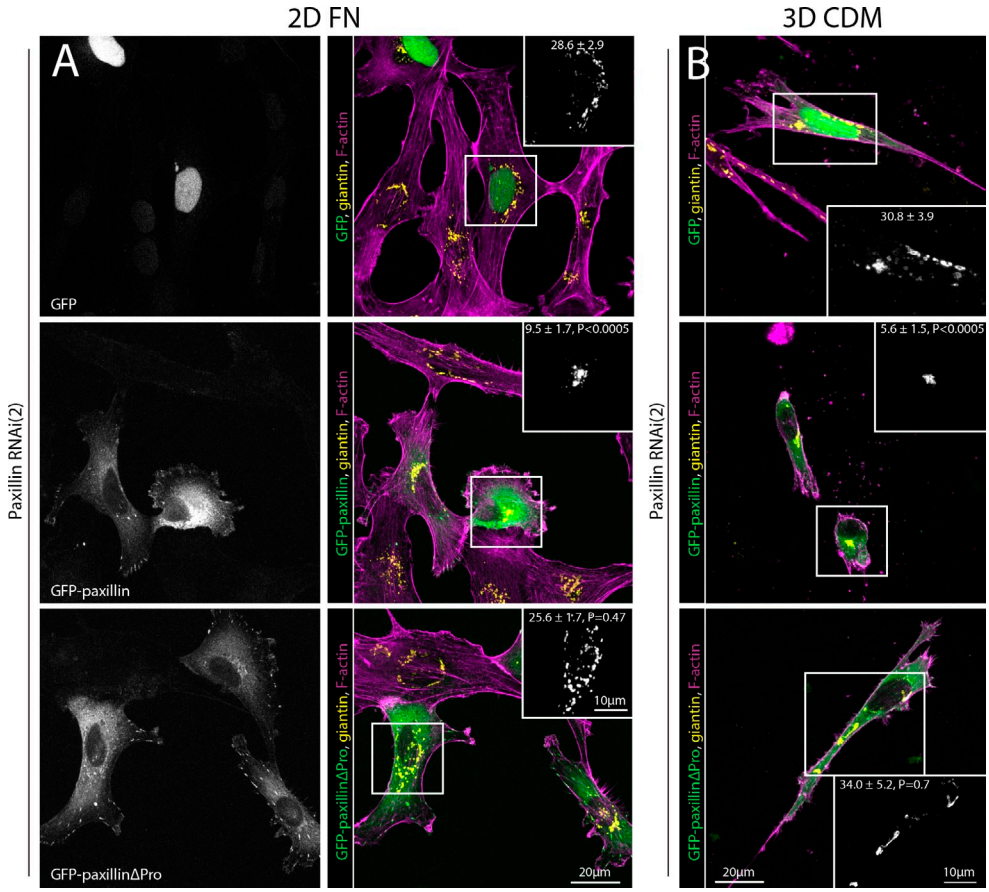

Figure 7. **Reexpression of a paxillin mutant lacking the proline-rich region is unable to rescue Golgi fragmentation and a motile phenotype.** (A and B) Images of MDA-MB-231 cells treated with paxillin RNAi, reexpressing GFP-tagged paxillin constructs as indicated spread on 2D fibronectin (FN; A) and 3D CDMs (B). The average number of Golgi objects/cell and statistical significance relative to the GFP control are indicated. *n* = minimum of 10 cells.

Having previously shown that paxillin regulates HDAC6 function through its proline-rich region (Fig. 4), we sought to determine whether this region of the protein was also essential for maintaining Golgi integrity. To test this requirement, paxillin-depleted MDA-MB-231 cells were transfected with RNAi-resistant GFP-tagged paxillin constructs. Reexpression of GFP-paxillin rescued Golgi cohesion in both 2D and 3D microenvironments (Fig. 7, A and B). Furthermore, GFP-paxillin expression also promoted rescue of the characteristic motile and polarized 3D phenotype of MDA-MB-231 cells (Fig. 7 B), rather than the hypermesenchymal, elongated morphology observed in untransfected paxillin RNAi-treated cells or cells expressing the GFP vector (Fig. 7 B), as described previously (Deakin and Turner, 2011). In contrast, reexpression of GFP-paxillinΔPro was unable to rescue either Golgi fragmentation or the nonmotile 3D cell morphology (Fig. 7, A and B). These data identify a novel role for the proline-rich region of paxillin in coordinating the cell polarization machinery, likely through its regulation of HDAC6-mediated MT acetylation-driven Golgi cohesion and positioning.

The requirement for MT acetylation in maintaining Golgi cohesion was confirmed by expression of a nonacetylatable K40R mutant of α-tubulin in parental MDA-MB-231 cells. Expression of this mutant, in contrast to wild-type GFP–α-tubulin, was sufficient to induce fragmentation of the Golgi apparatus in both 2D and 3D microenvironments (Fig. 8, A and B). Neither GFP–α-tubulin nor the K40R mutant caused any gross defects in the MT network (Fig. 8 C). In addition, expression of the α-tubulinK40R mutant, but not wild-type α-tubulin, promoted a more hyperelongated, bipolar morphology in cells migrating through 3D CDMs (Fig. 8, A and D). Importantly, both the 3D morphology and Golgi fragmentation observed in cells expressing α-tubulinK40R (Fig. 8, A and D) are also characteristic hallmarks of paxillin-depleted cells invading 3D ECM (Fig. 5 G and Fig. 6 F). In addition to α-tubulin, HDAC6 has other migration-relevant substrates, including cortactin and Hsp90 (Kovacs et al., 2005; Zhang et al., 2007), that may also be affected by paxillin regulation of HDAC6 activity. However, although these other HDAC6 substrates may play a role in cellular function, the GFP–α-tubulinK40R mutant data

area (D) of discrete Golgi objects per cell. (E) Western blots indicating no significant change in expression of the Golgi protein giantin in cells treated with paxillin RNAi. (F–H) Images (F) and quantitation of Golgi object number (G) and area in cells treated with RNAi (H) as stated. Where applicable, cells were treated with 2 μM tubacin 4 h before fixation. Data are represented as the mean ± SEM. **, P < 0.005; ***, P < 0.0005.

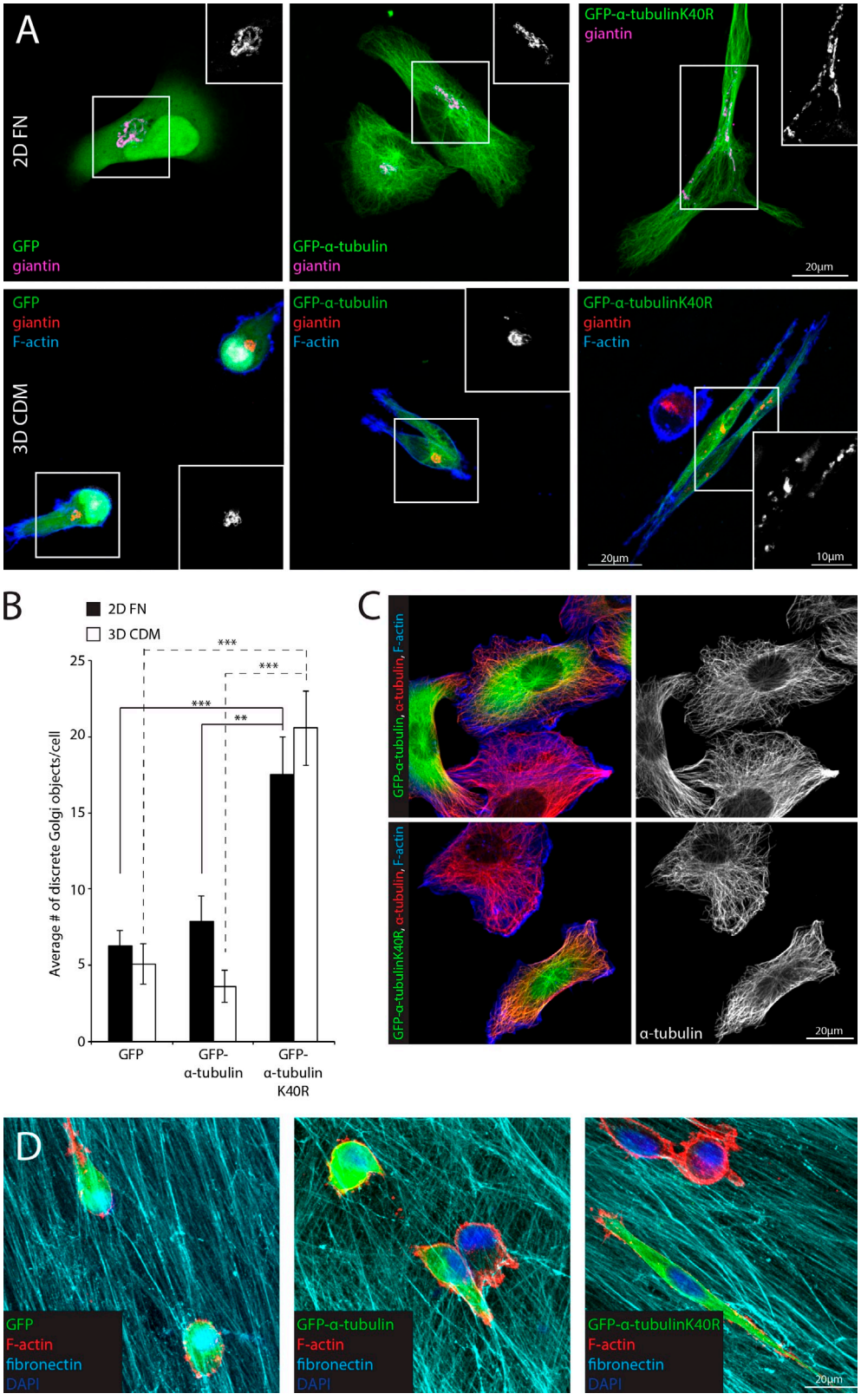

Figure 8. **Expression of the nonacetylatable α-tubulinK40R mutant is sufficient to promote Golgi fragmentation and a nonmotile paxillin RNAi-like 3D morphology.** (A and B) Images (A) and quantitation (B) of Golgi object number per cell in parental MDA-MB-231 cells expressing GFP-tagged constructs as indicated. Boxed regions indicate the area used for the respective zoomed giantin inset images. (C) Images to indicate that expression of either GFP-tagged α-tubulin construct has no gross effect on the overall MT network. (D) Representative images of MDA-MB-231 cells migrating through 3D CDMs indicating that, in contrast to the wild-type protein, GFP–α-tubulinK40R expression is sufficient to promote a nonmotile hyperelongated morphology. Data are from $n = 3$ individual repeats and represented as the mean ± SEM. **, $P < 0.005$; ***, $P < 0.0005$.

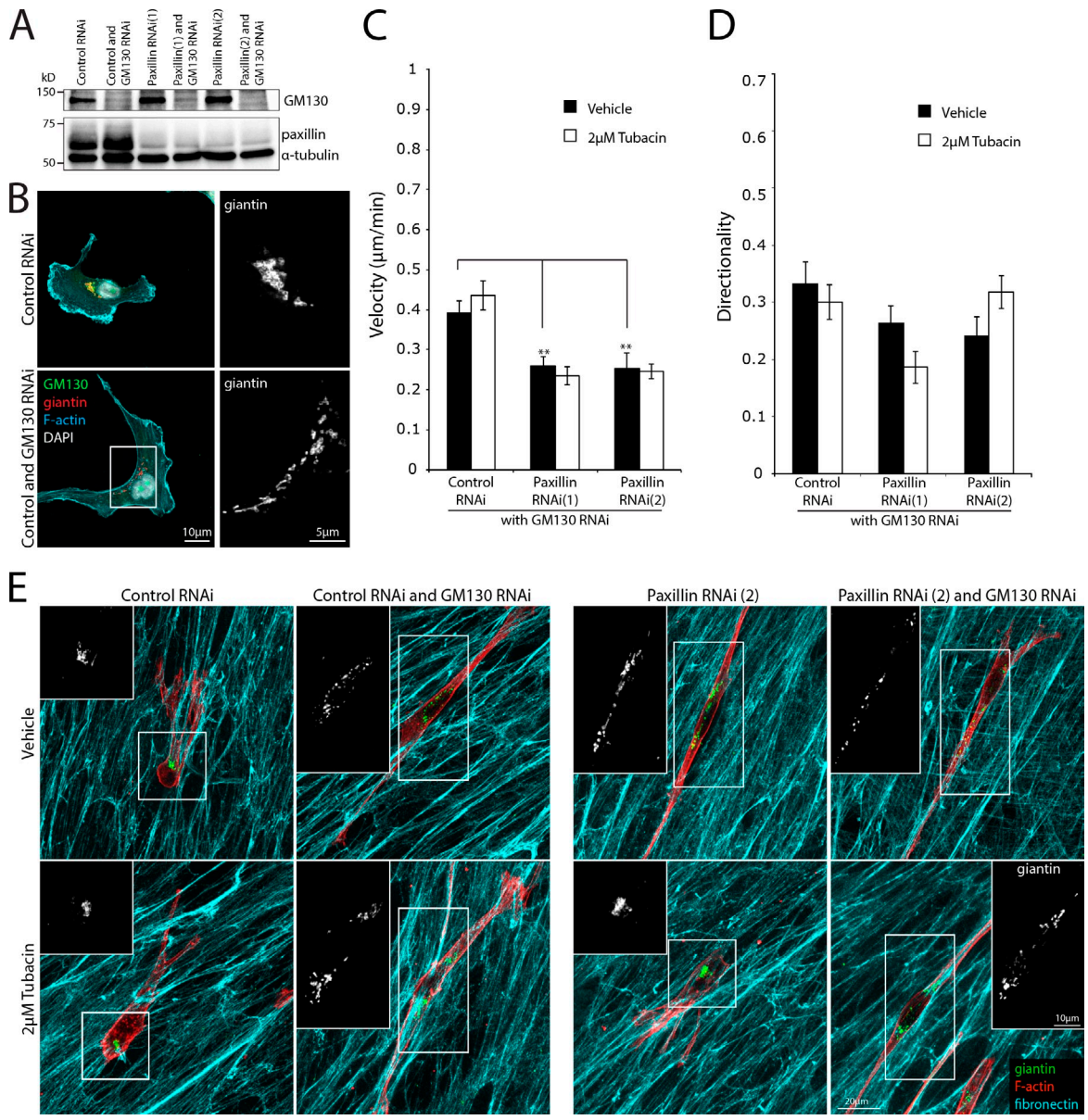

Figure 9. **HDAC6 inhibition rescues 3D motility in cells lacking paxillin and is dependent on Golgi cohesion.** (A) Western blot of paxillin and GM130 RNAi in MDA-MB-231 cells. (B) Images of MDA-MB-231 cells treated with GM130 RNAi. (C and D) Quantitation of migration velocity (C) and directionality of cells (D) treated with RNAi as indicated migrating through 3D CDMs. *n* = minimum of 25 cell tracks from three individual experiments. Data are represented as the mean ± SEM. **, P < 0.005. (E) Immunofluorescence images of the Golgi indicating that, in the absence of GM130, tubacin is unable to rescue the Golgi fragmentation or elongated cell morphology observed in cells lacking paxillin in 3D CDM. Boxed regions indicate the area used for the respective zoomed giantin inset images.

suggest that paxillin regulation of MT acetylation, via HDAC6, represents a critical signaling axis in the control of the cell polarization machinery.

To investigate whether there is a causal relationship between Golgi integrity and reorganization in the rescue of polarized motility in cells lacking paxillin, we performed RNAi-mediated knockdown of the Golgi membrane protein GM130 to block Golgi coalescence. Consistent with work by others (Puthenveedu et al., 2006), GM130 ablation (Fig. 9 A) resulted in Golgi fragmentation (Fig. 9, B and E). Importantly, depletion of GM130 in cells lacking paxillin prevented the tubacin-mediated rescue of polarized motility (Fig. 9, C and D; and see Fig. 5, D and E), suggesting that reorganization and cohesion of the Golgi is an absolute requirement for this process. Furthermore, despite the presence of acetylated MTs, GM130 depletion in control cells promoted a paxillin RNAi-like unpolarized, elongated 3D morphology (Fig. 9 E), highlighting the link between Golgi cohesion and the adoption of a polarized motile phenotype. As with polarized motility, HDAC6 inhibition with tubacin was unable to rescue either the polarized morphology or Golgi fragmentation in cells lacking both paxillin and GM130 (Fig. 9 E). These data therefore identify a fundamental role for paxillin as a key regulator of HDAC6 activity during the establishment and maintenance of a cohesive Golgi apparatus to enable polarized cell invasion and migration.

Discussion

MT acetylation is observed throughout organism development (Schatten et al., 1988) and is essential for a variety of fundamental cellular functions, including endocytosis (Montagnac et al., 2013), ciliogenesis (Pugacheva et al., 2007), and the migration of diverse cell types, such as neurons and endothelial cells (Creppe et al., 2009; Wang et al., 2010; Li et al., 2012). Additionally, enhanced MT acetylation in cancers results in cell cycle arrest, increased drug-induced apoptosis, and decreased tumor growth (Blagosklonny et al., 2002; Dowdy et al., 2006; Catalano et al., 2007) and as such is regarded as a positive prognostic factor. Therefore, understanding the mechanisms responsible for HDAC6 inhibition, which results in enhanced MT acetylation, is of paramount importance to cancer therapeutics. Data presented herein have identified a new and conserved role for paxillin as a key regulator of MT acetylation (Fig. 1). We have shown that paxillin depletion results in MT hypoacetylation (Fig. 1), indicating that paxillin functions to promote MT acetylation. Furthermore, this appears to be a nonredundant role for paxillin, as despite extensive functional cross talk, structural homology, and shared interacting proteins (Brown and Turner, 2004), RNAi-mediated depletion of the paxillin family member Hic-5 had no significant effect on MT acetylation (Fig. 1 B).

Historically, paxillin has been shown to elicit its effects on cell adhesion and migration through its ability to localize to sites of integrin-mediated cell attachment to the ECM in both 2D and 3D matrix microenvironments (Brown and Turner, 2004; Deakin and Turner, 2008, 2011). However, HDAC6 is not strongly enriched in FAs and instead is widely distributed throughout the cytosol (Fig. 3 E), with some reported enrichment on MTs and at the leading edge of migrating cells (Hubbert et al., 2002). Moreover, HDAC6 has also been shown to have potent deacetylase activity toward assembled MTs rather than soluble α-tubulin (Hubbert et al., 2002). However, the precise spatiotemporal activation of HDAC6 and thus MT deacetylation remains enigmatic. Interestingly, we found that after washout of the HDAC6 inhibitor tubacin, the resulting deacetylation of MTs was largely restricted to the leading edge of membrane protrusion in control cells (Fig. 2 E). In stark contrast, cells lacking paxillin displayed a significantly enhanced rate of HDAC6-dependent global MT deacetylation (Fig. 2, C–E), with no apparent effect on total acetyltransferase activity (Fig. 2, F and G). Using PLA, apFRET, and co-IP, we determined that HDAC6 and paxillin exist in a complex, which is distributed throughout the cell (Fig. 3) and is dependent on the proline-rich region of paxillin (Fig. 4, D–F). Our analyses also revealed that a small percentage of the paxillin–HDAC6 complex was consistently observed juxtaposed to and coincident with larger FAs (Fig. 3, E and H). It is interesting to speculate that the paxillin–HDAC6 complexes located throughout the cell may be necessary for the global regulation of MT acetylation and thus may impact trafficking from the Golgi to the plasma membrane. In contrast, those paxillin–HDAC6 complexes observed in the vicinity of FAs may be required for the localized regulation of MT stability and/or adhesion targeting and thereby may be more important in regulating the dynamics of FAs. Indeed, it has been previously shown that displacement of paxillin from adhesion structures to the cytosol, through overexpression of paxillin LIM2-LIM3 domains, results in an increase in MT stability at FAs (Efimov et al., 2008). It will be of interest in future studies to dissect the respective roles of these potentially distinct pools of paxillin–HDAC6 complexes.

It is of note that we frequently observed the most robust PLA signal between paxillin and HDAC6 in cells with large stress fibers (Fig. 3 A, cells with asterisks). Both the formation of stress fibers and large adhesions are linked to and induced by the activation of RhoA (Chrzanowska-Wodnicka and Burridge, 1996). Therefore, it is plausible that RhoA activation may promote the association of paxillin and HDAC6 and thus result in HDAC6 inhibition and concomitant enhanced MT acetylation. Indeed, we have previously shown that activation of RhoA can dictate the spatial distribution of paxillin's interactome (Deakin et al., 2012). For example, RhoA activation leads to an increase in paxillin association with inactive vinculin in the cell cytosol/membrane and enhances its association with actopaxin in adhesions (Deakin et al., 2012). Furthermore, FAK-mediated activation of RhoA has been shown to stimulate MT acetylation (Palazzo et al., 2004), consistent with a role for this signaling axis in HDAC6 inhibition. Whether paxillin activates RhoA, via its association with FAK to stimulate its interaction with HDAC6, or alternatively, whether the association of paxillin and HDAC6 leads to FAK and RhoA activation remains to be determined. However, it is noteworthy that paxillin depletion results in decreases in both active FAK and RhoA levels (Deakin and Turner, 2011) as well as enhanced HDAC6 activation (Fig. 2), which suggests that these signaling axes may be integrated by paxillin to spatiotemporally coordinate both the MT and the actin cytoskeleton.

Although our interaction data are indicative (Fig. 3), it remains to be determined whether paxillin interacts directly with HDAC6. Nevertheless, our domain mapping analysis identified a clear role for the proline-rich region of paxillin in mediating the paxillin–HDAC6 association (Fig. 4, D–F) as well as HDAC6 inactivation to regulate MT acetylation (Fig. 4, B and C) and Golgi cohesion (Fig. 7). It is of interest that other class II HDAC family members can be also regulated by their interaction with proline-rich regions of proteins. For example, both HDAC7 and 9 have been shown to interact with the proline-rich region of the FOXP3 to activate its activity as a transcriptional repressor (Li et al., 2007).

Tumor cell invasion and associated metastasis is considered the single worst prognostic factor in cancer progression. Overexpression and activation of HDAC6 promotes both cell transformation and invasion through inducing MT hypoacetylation (Hubbert et al., 2002; Tran et al., 2007; Lee et al., 2008; Williams et al., 2013). Consistent with a previous study (Rey et al., 2011), HDAC6 inhibition by tubacin or through RNAi-mediated protein depletion inhibited MDA-MB-231 cell invasion (Fig. 5, A and B) as well as HFF and Hs578T wound closure (Fig. S1). In contrast, the inhibition of HDAC6 in paxillin-depleted cells resulted in enhanced invasive capacity of MDA-MB-231 cells (Fig. 5) and an increase in directional migration of HFF and Hs578T cells (Fig. S1) to a level comparable to HDAC6-inhibited control cells. These data suggest that the hypoacetylation

observed in paxillin-depleted cells, resulting from HDAC6 activation, is at least in part responsible for their decreased motility. Similar results have also been observed in the developing cerebral cortex after silencing the Elongator acetyltransferase complex, in which rescuing MT hypoacetylation with tubacin promoted cortical neuron migration (Creppe et al., 2009). The data presented herein suggest that, although a balance of MT acetylation and deacetylation results in optimal invasion, α-tubulin acetylation is able to rescue the cell motility machinery in paxillin-depleted cells.

Previous studies have shown that paxillin is necessary for cancer cell invasion through its regulation of invadopodia, 3D adhesion dynamics, and the ability of cancer cells to switch between amoeboid and mesenchymal modes of motility (Bowden et al., 1999; Deakin and Turner, 2011). Importantly, all of these processes also involve dynamic regulation and acetylation of the MT cytoskeleton. In the case of adhesion dynamics, the targeting of MTs to integrin-mediated adhesions is necessary for their disassembly (Kaverina et al., 1999), and this can be regulated by paxillin (Efimov et al., 2008). Tightly controlled adhesion assembly, stabilization, and disassembly are an absolute requirement for efficient and productive mesenchymal cell migration (Kaverina et al., 2002). Therefore, the rescue of motility in tubacin-treated paxillin-depleted cells suggests that HDAC6 regulation by paxillin contributes to the control of adhesion dynamics. We have previously shown that paxillin depletion promotes a nonmotile hypermesenchymal phenotype of breast cancer cells seeded in 3D ECMs and prevents their transition to an amoeboid mode of motility (Deakin and Turner, 2011). Thus, the inability of cells to exhibit productive mesenchymal motility upon paxillin depletion may be caused by their lack of stable acetylated MTs, which has been shown to facilitate this mode of migration (Belletti et al., 2008).

A further consequence of paxillin depletion is the loss of cell polarization, which in 3D ECMs is characterized by a loss of correlation between cell front protrusion and rear retraction (Deakin and Turner, 2011) and a decrease in persistent migration (Fig. 5, C and E). Herein, we observed that this loss of polarized motility and fragmentation of the Golgi in paxillin-depleted cells can both be rescued by HDAC6 inhibition (Fig. 6). Several substrates of HDAC6, including cortactin and Hsp90 (Kovacs et al., 2005; Zhang et al., 2007) influence cell migration, and thus, their hypoacetylation may be involved in the nonmotile phenotype of cells lacking paxillin. However, similar to paxillin depletion, expression of a nonacetylatable K40R mutant of α-tubulin was sufficient to induce Golgi dispersion and a nonmotile phenotype (Fig. 8), which suggests a causal role for MT acetylation in these processes. Importantly, overexpression of the α-tubulinK40R in other cell types has also been shown to perturb directional motility (Li et al., 2012), in part through inhibition of polarized kinesin-1–mediated trafficking (Reed et al., 2006). Interestingly, kinesin-1 binding and trafficking is enhanced upon MT acetylation (Reed et al., 2006), and this motor protein is essential for both the delivery of polarity proteins to the correct locale (Hurd and Saxton, 1996; Ling et al., 2004; League and Nam, 2011) as well as the MT-mediated dissolution of FAs (Krylyshkina et al., 2002). Given the loss of MT acetylation in cells lacking paxillin, it is possible that the observed defects in cell polarization and migration may be caused in part by dysfunction of kinesin-1–driven processes.

Fragmentation of the Golgi after GM130 RNAi also promoted a nonmotile paxillin RNAi-like morphology, which could not be rescued by HDAC6 inhibition irrespective of paxillin expression (Fig. 9, C–E). Importantly, GM130 depletion does not influence MT acetylation (unpublished data). Collectively, we conclude that paxillin-mediated control of MT acetylation is required to regulate Golgi cohesion, which in turn is an absolute requirement for 3D cell morphology as well as polarized migration. Despite the previously observed enrichment of acetylated MTs at the Golgi apparatus (Thyberg and Moskalewski, 1993), we believe that this is the first direct evidence that MT acetylation is required for and indeed drives Golgi cohesion and maintenance (Fig. 6 and Fig. 8). Furthermore, we have shown that paxillin-mediated inhibition of HDAC6 is essential for the maintenance of Golgi integrity in both normal and malignant cell types (Fig. 6 and Fig. S3). Whether enhanced MT acetylation regulates Golgi structure through providing a stable scaffold as a result of their increased longevity or whether the enhanced kinesin-1–mediated motor activity is the driving force behind Golgi stack integration remains to be determined. It is noteworthy, however, that MT destabilization and dissolution is a prerequisite for Golgi fragmentation during mitosis (Thyberg and Moskalewski, 1999), and kinesin-1 both localizes to and is essential for Golgi maintenance (Lippincott-Schwartz et al., 1995). Further research is necessary, but it is likely that both MT stability and kinesin motor function combine to facilitate Golgi structure and function.

In conclusion, the data presented herein identify a new role for paxillin as a fundamental regulator of MT acetylation via an inhibitory interaction with HDAC6. Furthermore, we have shown that paxillin-mediated inhibition of HDAC6 is required to regulate the integrity of the Golgi apparatus as well as polarized cell motility in both 2D and 3D microenvironments.

Materials and methods

Cell lines, reagents, and antibodies

The paxillin-null (paxillin$^{-/-}$) MEFs were a gift from S. Thomas (Harvard Medical School, Cambridge, MA) and have been described previously. The constitutive paxillin knockout was achieved by replacing the 1.6-kb genomic sequence encoding exons 2 and 3 of mouse paxillin with a promoterless β-galactosidase–neomycin cassette (Hagel et al., 2002). MDA-MB-231, Hs578T, HFF, and NIH-3T3 cell lines were purchased from the ATCC and maintained in complete growth media. The NIH-3T3 cells were cultured in DMEM containing 10% (vol/vol) calf serum supplemented with 2 mM L-glutamine, 1 mM sodium pyruvate, and 1% (vol/vol) penicillin and streptomycin. All other cell lines were cultured in DMEM supplemented as stated here containing 10% (vol/vol) fetal bovine serum and were maintained in a 37°C humidified chamber with 5% CO_2.

Antibodies used in this study include mouse anti-paxillin (clones 349 and 165 for Western blotting and immunofluorescence, respectively), mouse anti-GM130, mouse anti-fibronectin (BD), mouse anti–acetylated α-tubulin (clone 6-11B-1), mouse anti–α-tubulin (clone DM1A), mouse anti–α-actinin, rabbit anti-fibronectin, rabbit anti-HDAC6 (Sigma-Aldrich), rabbit anti-paxillin, normal mouse IgG (Santa Cruz Biotechnology, Inc.), rabbit anti-tubulin, rabbit anti-HDAC6 (Abcam), mouse anti-SIRT2 (Cell Signaling Technology), mouse anti-actin (EMD Millipore), and rabbit anti-giantin (Covance). Rhodamine- and Alexa Fluor 488–conjugated phalloidin (Life Technologies) and DAPI (Sigma-Aldrich) were used for fluorescent detection of F-actin and the cell nucleus, respectively. Anti–mouse and anti–rabbit Dylight 488– and 633–conjugated antibodies were used for all immunofluorescence

experiments (Thermo Fisher Scientific). Tubacin was purchased from Sigma-Aldrich and was used at a concentration of 2 µM, with cells treated for 4 h before fixation unless otherwise stated.

RNAi and transfections

Where indicated, cells were transfected with siRNAs for 72 h, unless stated otherwise, using Oligofectamine (Life Technologies) following the manufacturer's instructions and using a concentration of 0.1 µM for each oligonucleotide (oligo). The paxillin RNAi(1) was purchased from Thermo Fisher Scientific (catalog number Custom0008), and all other siRNA oligos used were purchased from Life Technologies (catalog number AM16106) without modifications. The human siRNA sequences were as follows: paxillin RNAi(1), 5′-CCCUGACGAAAGAGAAGCCUA-3′ and 5′-UAGGCUUCUCUUUCGUCAGGG-3′; paxillin RNAi(2), 5′-GUGUGGAGCCUUCUUUGGU-3′ and 5′-ACCAAAGAAGGCUCCACAC-3′; Hic-5 RNAi, 5′-GGACCAGUCUGAAGAUAAG-3′ (Deakin and Turner, 2011); HDAC6 RNAi, 5′-CAUCCAAGUCCAUCGCAGAUU-3′ and 5′-UCUGCGAUGGACUUGGAUGUU-3′ (Kaluza et al., 2011); GM130 RNAi, 5′-GUUAGAGAUGACGGAACUCTT-3′ and 5′-GAGUUCCGUCAUCUCUCUAACTT-3′ (Puthenveedu et al., 2006); SIRT2 RNAi, 5′-GGAGCUGGAAUCUCCACAUTT-3′ and 5′-AUGUGGAGAUUCCAGCUCCTT-3′; and control RNAi, 5′-ACUCUAUCUGCACGCUGACUU-3′ and 5′-GUCAGCGUGCAGAUAGAGUUU-3′. The control nonspecific siRNA was used in all experiments as indicated. The efficiency of paxillin knockdown was routinely assessed by Western blotting and was 92.6 ± 0.96% and 93.2 ± 1.2% for RNAi oligos 1 and 2, respectively. Depletion of Hic-5, a paxillin family member, had no significant effect on α-tubulin acetylation.

Cells were transiently transfected with EGFP, EGFP-paxillin, EGFP-paxillin mutants, and EGFP–α-tubulinK40R using Lipofectamine LTX (Life Technologies) following the manufacturer's standard instructions. For knockdown and reexpression experiments, cells were treated with paxillin RNAi(2) as in the previous paragraph for 48 h before transfection with cDNA as stated using a transfection system (TransIT-X2 Dynamic Delivery System; Mirus Bio LLC) following the standard manufacturer's instructions. Cells were left for 24 h after transfection before cell spreading and fixation.

Immunofluorescence microscopy

Glass coverslips were coated with fibronectin at 10 µg/ml for 16 h at 4°C in PBS containing magnesium, and calcium or 3D CDMs were grown on 12-mm glass coverslips as described for 3D analyses. Coverslips (both 2D and 3D) were blocked with heat-denatured BSA at 10 mg/ml. MDA-MB-231 cells, in complete growth medium at 5×10^4 cells/ml, were incubated on 2D or 3D coverslips for 16 h at 37°C, unless otherwise stated. Cells were washed once in PBS, fixed, and permeabilized simultaneously using 1% glutaraldehyde with 1% (vol/vol) Triton X-100 in PBS, quenched with 1% (wt/vol) $NaBH_4$ in PBS, and then blocked overnight at 4°C with 3% (wt/vol) BSA. Fixed cells were stained with primary antibodies as indicated. PBS with 0.05% Tween 20 was used for subsequent washes. Cells were imaged using a scanning confocal microscope (SP5; Leica) with a HCX Plan Apochromat 63×/1.40–0.60 NA oil λ blue objective and associated hybrid and standard photomultiplier tube detectors. Images were acquired using the LAS AF (Leica Application Suite Advanced Fluorescence) software (Leica).

PLAs

PLAs were performed following the manufacturer's instructions using the Duolink anti–Mouse MINUS and anti–Rabbit PLUS In Situ PLA probes and the Duolink In Situ Detection Reagents Red (Olink Bioscience). Cells were counterstained with Alexa Fluor 488–conjugated phalloidin and DAPI and imaged using the scanning confocal (SP5) with a HCX Plan Apochromat 63×/1.40–0.60 NA oil λ blue objective. To determine PLA proximity to adhesion contacts, cells were infected with talin-GFP baculovirus (CellLight; Life Technologies) 24 h before fixation, and PLA was infected with the indicated antibody pairs.

apFRET

apFRET experiments were performed and quantified as previously described (Deakin et al., 2009, 2012). Paxillin-null MEFs were transfected with a cDNA ratio of 2:1 donor to acceptor. 16 h after transfection, cells were plated on 10 µg/ml fibronectin-coated 35-mm glass-bottomed, poly-L-lysine dishes (MatTek Corporation), which had been blocked with 10 mg/ml heat-denatured BSA for 30 min. Forty thousand cells were added to each well and allowed to attach and spread overnight at 37°C with 5% (vol/vol) CO_2. The spread cells were then fixed for 15 min at room temperature with 4% (wt/vol) paraformaldehyde in PBS, washed with PBS, and then quenched with 0.1 M glycine in PBS for 15 min at room temperature before storage in distilled H_20 for imaging. Fixed cells were imaged in the GFP and RFP channel on a deconvolution microscope (AF6000 LX; Leica) and LAS AF software using a 100×/1.40–0.70 NA HCX Plan Apochromat objective (Leica) and electron-multiplying charge-coupled device camera (Luca R; Andor Technology). A GFP image (donor) was captured before and after photobleaching the mRFP (acceptor). To control for pixel shift aberrations and edge artifacts, the GFP images taken before and after photobleaching were merged, and pixel alignment fidelity was assessed and corrected. After image-specific background subtraction, the percentage of FRET efficiency was calculated on a pixel-by-pixel basis as 100 × [1 − (donor intensity before photobleaching/donor intensity after photobleaching)] using ImageJ software (National Institutes of Health). FRET images were smoothed and displayed as a color intensity scale.

Co-IP assays and immunoblots

For each co-IP, 1.6×10^6 cells were plated overnight in serum on 10 µg/ml fibronectin-coated 10-cm dishes, and then after a brief PBS wash at 4°C, lysates were prepared using 400 µl of ice-cold extraction buffer containing 50 mM Hepes, pH 7.4, 150 mM NaCl, 1% (vol/vol) Triton X-100, 1% (wt/vol) sodium deoxycholate, 0.1% (wt/vol) SDS, and 10% (vol/vol) glycerol supplemented with inhibitor cocktail (1 mM PMSF, 20 µg/ml leupeptin, 5 µM cytochalasin D, and 5 µM latrunculin A). After 10 min of cell lysis on ice in the extraction buffer, samples were collected and centrifuged at 6,000 *g* for 10 min at 4°C. Supernatants were then diluted twofold in ice-cold HNTG buffer containing 50 mM Hepes, pH 7.4, 150 mM NaCl, 0.1% (vol/vol) Triton X-100, and 10% (vol/vol) glycerol supplemented with inhibitor cocktail. Samples were then incubated rotating at 4°C with 1 µg of antibody as indicated for 1 h before the addition of protein A/G beads for a further 30 min. The beads were collected and washed twice with 500 µl ice-cold HNTG buffer before SDS-PAGE analysis. Western blots were visualized using enhanced chemiluminescence substrate (SuperSignal West; Thermo Fisher Scientific) and an imaging system (ChemiDoc MP; Bio-Rad Laboratories). Knockdown efficiency was assessed routinely with protein-specific antibodies for each experiment. Where stated, band intensity was quantified using ImageLab software (Bio-Rad Laboratories).

HDAC6 activation and acetyltransferase activity assays

To quantify HDAC6 activity, MDA-MB-231 cells were treated with 2 µM tubacin for 16 h in complete growth medium to ensure maximal MT acetylation, which was confirmed through both Western blotting and immunofluorescence. The medium containing the inhibitor was then removed and replaced with complete growth medium. Total cell lysates were prepared at the time points stated by addition of hot reducing sample buffer and analyzed by Western blotting and band densitometry. The rate of α-tubulin deacetylation was determined by quantitation of the acetylated α-tubulin band intensity versus time relative to the α-tubulin and α-actinin loading controls, which was analyzed using Excel (Microsoft). In order to assess acetyltransferase activity, cell lysates were created at the stated time point after tubacin addition, and α-tubulin acetylation was determined by Western blotting.

Inverted invasion assay

The inverted collagen and fibronectin invasion assay was performed as described previously (Deakin and Turner, 2011). In brief, collagen I (PureCol; Advanced BioMatrix), mixed 5:1 with 10× MEM, supplemented with 25 µg/ml fibronectin, was allowed to polymerize in 8-µm pore size transwell inserts (Corning) for 1 h at 37°C in the absence of CO_2. MDA-MB-231 cells treated with siRNA oligos as stated for 24 h were resuspended in serum-free medium and 10^5 cells/ml and were seeded on the inverted transwell, on the filter surface. Cells were allowed to adhere for 1 h at 37°C in the presence of CO_2. Transwells were then placed in 1 ml serum-free medium, with the addition of 2 µM tubacin where stated. To establish a chemotactic gradient, medium supplemented with 10% fetal bovine serum and inhibitors where stated was placed in the upper chamber of the transwell. 4 d after seeding, cells were stained with Calcein AM (Life Technologies) and visualized using the HC Plan Apochromat 20×/0.70 NA immersion correction collar λ blue objective (Leica) and laser-scanning confocal microscopy (SP5). Images were acquired in 10-µm intervals up to 150 µm from the transwell surface as determined by phase-contrast imaging. Total cells in all images of the confocal series were quantified using ImageJ, and the relative percentage of cells invading ≥40 µm into the collagen and fibronectin plug was determined.

3D CDM generation and 3D migration analysis

3D CDMs were generated as previously described (Deakin and Turner, 2011). In brief, 6-well plates (CELLTREAT Scientific Products), glass-bottom dishes (MatTek Corporation), and glass coverslips were coated with 0.2%

sterile gelatin for 30 min at 37°C. Glass-bottom dishes and glass coverslips were subsequently treated with 1% glutaraldehyde (vol/vol) to cross-link the gelatin and then quenched with 1 M glycine. After incubation with complete growth medium, 10^5 cells/ml of primary HFFs were seeded onto each dish and cultured for 10–14 d. Cell growth medium was changed every 2 d and supplemented with 50 µg/ml ascorbic acid to stabilize the collagen matrix. The matrices were denuded of cells by treating the cell monolayers with 20 mM NH_4OH, 0.5% Triton X-100 (vol/vol), and PBS for 2 min at 37°C. CDMs were then washed repeatedly and stored in cold PBS containing magnesium and calcium.

Parental or siRNA-treated MDA-MB-231 cells as indicated were allowed to spread on CDMs for 4 h in the presence of serum (with or without vehicle or inhibitors as indicated) before imaging. Time-lapse imaging was performed on a microscope (TE2000; Nikon) equipped with an environmental chamber with images acquired every 10 min for 16 h using a HCX Plan Fluotar 10×/0.30 NA objective and Elements software (Nikon). ImageJ software was used to track cell centroid movement and to calculate migration velocity and directionality of all cells present in the field throughout the time course. The persistence was calculated as previously described (Pankov et al., 2005; Deakin and Turner, 2011) using the manual tracking and chemotaxis tool plugins for ImageJ. Tracks were derived from raw data points and were plotted in Excel.

Wound-healing assay

Hs578T or HFF cells were treated with siRNA for 24 h before seeding at high density in 6-well plates (5×10^5 cells/well). Cells were left to spread and reach confluence for 24 h before wounding. Monolayers were scraped using a pipette tip and washed four times with prewarmed complete growth medium. The wounded monolayer was treated with vehicle or 2 µM tubacin as indicated and was then imaged using a microscope (TE2000) equipped with a 10× objective, and images were taken every 10 min for 24 h. Nuclei of cells at the wound edge were tracked manually, and directionality was measured using the manual tracking and chemotaxis tool plugins in ImageJ.

Image quantitation and Golgi morphometric analyses

To determine mean fluorescence intensity (MFI), representative images were background subtracted and thresholded for particles with values between 20 and 256 before quantitation using the analyze particles plugin in ImageJ. Values were made relative to the GFP control. MFI was measured from a minimum of 20 cells from three independent experiments. Costes' randomization was quantified for 12 representative background-subtracted images of talin-GFP and PLA spots using 200 iterations using the JACoP (Just Another Colocalization Plugin) plugin for ImageJ. A value of >95% indicated a positive correlation between the channels (Costes et al., 2004). For Golgi morphometric analyses, representative images were background subtracted, and Golgi area, object number, and object area were quantified using the analyze particles plugin in ImageJ.

Statistical analyses

Two-tailed unpaired Student's *t* tests were used for all statistical analyses between two groups using Excel. Statistical analyses between multiple groups were assessed using a one-way analysis of variance followed by a Dunnett's post hoc test and performed using Prism software (GraphPad Software).

Online supplemental material

Fig. S1 demonstrates that polarized motility and MT acetylation is decreased in both Hs578T cells and HFFs lacking paxillin expression, as assessed using a wound-healing assay (Fig. 1, Fig. 2, and Fig. 5). The immunofluorescence images displayed in Fig. S2 indicate that the loss of MT acetylation in paxillin-depleted MDA-MB-231 cells can be rescued by HDAC6 inhibition or protein depletion (Fig. 2). Fig. S3 displays representative images of the Golgi fragmentation phenotype observed in both normal and transformed cells treated with paxillin RNAi (Fig. 6). Fig. S4 demonstrates that the Golgi fragmentation induced by paxillin RNAi can be rescued by both HDAC6 RNAi as well as treatment with the HDAC6-specific inhibitor tubacin (Fig. 6). Online supplemental material is available at http://www.jcb.org/cgi/content/full/jcb.201403039/DC1. Additional data are available in the JCB DataViewer at http://dx.doi.org/10.1083/jcb.201403039.dv.

We would like to thank past and present members of the Turner Lab for insightful discussion of data.

This work was supported by National Institutes of Health grants RO1CA163296 and RO1GM47607 (to C.E. Turner).

The authors declare no competing financial interests.

Submitted: 10 March 2014
Accepted: 26 June 2014

References

Akella, J.S., D. Wloga, J. Kim, N.G. Starostina, S. Lyons-Abbott, N.S. Morrissette, S.T. Dougan, E.T. Kipreos, and J. Gaertig. 2010. MEC-17 is an alpha-tubulin acetyltransferase. *Nature*. 467:218–222. http://dx.doi.org/10.1038/nature09324

Aldana-Masangkay, G.I., and K.M. Sakamoto. 2011. The role of HDAC6 in cancer. *J. Biomed. Biotechnol.* 2011:1–10. http://dx.doi.org/10.1155/2011/875824

Belletti, B., M.S. Nicoloso, M. Schiappacassi, S. Berton, F. Lovat, K. Wolf, V. Canzonieri, S. D'Andrea, A. Zucchetto, P. Friedl, et al. 2008. Stathmin activity influences sarcoma cell shape, motility, and metastatic potential. *Mol. Biol. Cell*. 19:2003–2013. http://dx.doi.org/10.1091/mbc.E07-09-0894

Bergmann, J.E., A. Kupfer, and S.J. Singer. 1983. Membrane insertion at the leading edge of motile fibroblasts. *Proc. Natl. Acad. Sci. USA*. 80:1367–1371. http://dx.doi.org/10.1073/pnas.80.5.1367

Bisel, B., Y. Wang, J.H. Wei, Y. Xiang, D. Tang, M. Miron-Mendoza, S. Yoshimura, N. Nakamura, and J. Seemann. 2008. ERK regulates Golgi and centrosome orientation towards the leading edge through GRASP65. *J. Cell Biol.* 182:837–843. http://dx.doi.org/10.1083/jcb.200805045

Blagosklonny, M.V., R. Robey, D.L. Sackett, L. Du, F. Traganos, Z. Darzynkiewicz, T. Fojo, and S.E. Bates. 2002. Histone deacetylase inhibitors all induce p21 but differentially cause tubulin acetylation, mitotic arrest, and cytotoxicity. *Mol. Cancer Ther.* 1:937–941.

Bobrowska, A., G. Donmez, A. Weiss, L. Guarente, and G. Bates. 2012. SIRT2 ablation has no effect on tubulin acetylation in brain, cholesterol biosynthesis or the progression of Huntington's disease phenotypes in vivo. *PLoS ONE*. 7:e34805. http://dx.doi.org/10.1371/journal.pone.0034805

Bowden, E.T., M. Barth, D. Thomas, R.I. Glazer, and S.C. Mueller. 1999. An invasion-related complex of cortactin, paxillin and PKCmu associates with invadopodia at sites of extracellular matrix degradation. *Oncogene*. 18:4440–4449. http://dx.doi.org/10.1038/sj.onc.1202827

Brown, M.C., and C.E. Turner. 2002. Roles for the tubulin- and PTP-PEST-binding paxillin LIM domains in cell adhesion and motility. *Int. J. Biochem. Cell Biol.* 34:855–863. http://dx.doi.org/10.1016/S1357-2725(01)00154-6

Brown, M.C., and C.E. Turner. 2004. Paxillin: adapting to change. *Physiol. Rev.* 84:1315–1339. http://dx.doi.org/10.1152/physrev.00002.2004

Burkhardt, J.K. 1998. The role of microtubule-based motor proteins in maintaining the structure and function of the Golgi complex. *Biochim. Biophys. Acta*. 1404:113–126. http://dx.doi.org/10.1016/S0167-4889(98)00052-4

Cabrero, J.R., J.M. Serrador, O. Barreiro, M. Mittelbrunn, S. Naranjo-Suárez, N. Martín-Cófreces, M. Vicente-Manzanares, R. Mazitschek, J.E. Bradner, J. Avila, et al. 2006. Lymphocyte chemotaxis is regulated by histone deacetylase 6, independently of its deacetylase activity. *Mol. Biol. Cell*. 17:3435–3445. http://dx.doi.org/10.1091/mbc.E06-01-0008

Cambray-Deakin, M.A., and R.D. Burgoyne. 1987. Acetylated and detyrosinated alpha-tubulins are co-localized in stable microtubules in rat meningeal fibroblasts. *Cell Motil. Cytoskeleton*. 8:284–291. http://dx.doi.org/10.1002/cm.970080309

Catalano, M.G., R. Poli, M. Pugliese, N. Fortunati, and G. Boccuzzi. 2007. Valproic acid enhances tubulin acetylation and apoptotic activity of paclitaxel on anaplastic thyroid cancer cell lines. *Endocr. Relat. Cancer*. 14:839–845. http://dx.doi.org/10.1677/ERC-07-0096

Chen, C.S., S.C. Weng, P.H. Tseng, H.P. Lin, and C.S. Chen. 2005. Histone acetylation-independent effect of histone deacetylase inhibitors on Akt through the reshuffling of protein phosphatase 1 complexes. *J. Biol. Chem.* 280:38879–38887. http://dx.doi.org/10.1074/jbc.M505733200

Chen, S., G.C. Owens, H. Makarenkova, and D.B. Edelman. 2010. HDAC6 regulates mitochondrial transport in hippocampal neurons. *PLoS ONE*. 5:e10848. http://dx.doi.org/10.1371/journal.pone.0010848

Chrzanowska-Wodnicka, M., and K. Burridge. 1996. Rho-stimulated contractility drives the formation of stress fibers and focal adhesions. *J. Cell Biol.* 133:1403–1415. http://dx.doi.org/10.1083/jcb.133.6.1403

Costes, S.V., D. Daelemans, E.H. Cho, Z. Dobbin, G. Pavlakis, and S. Lockett. 2004. Automatic and quantitative measurement of protein-protein colocalization in live cells. *Biophys. J.* 86:3993–4003. http://dx.doi.org/10.1529/biophysj.103.038422

Creppe, C., L. Malinouskaya, M.L. Volvert, M. Gillard, P. Close, O. Malaise, S. Laguesse, I. Cornez, S. Rahmouni, S. Ormenese, et al. 2009. Elongator controls the migration and differentiation of cortical neurons through acetylation of alpha-tubulin. *Cell*. 136:551–564. http://dx.doi.org/10.1016/j.cell.2008.11.043

Cukierman, E., R. Pankov, D.R. Stevens, and K.M. Yamada. 2001. Taking cell-matrix adhesions to the third dimension. *Science*. 294:1708–1712. http://dx.doi.org/10.1126/science.1064829

Deakin, N.O., and C.E. Turner. 2008. Paxillin comes of age. *J. Cell Sci.* 121:2435–2444. http://dx.doi.org/10.1242/jcs.018044

Deakin, N.O., and C.E. Turner. 2011. Distinct roles for paxillin and Hic-5 in regulating breast cancer cell morphology, invasion, and metastasis. *Mol. Biol. Cell*. 22:327–341. http://dx.doi.org/10.1091/mbc.E10-09-0790

Deakin, N.O., M.D. Bass, S. Warwood, J. Schoelermann, Z. Mostafavi-Pour, D. Knight, C. Ballestrem, and M.J. Humphries. 2009. An integrin-alpha4-14-3-3zeta-paxillin ternary complex mediates localised Cdc42 activity and accelerates cell migration. *J. Cell Sci.* 122:1654–1664. http://dx.doi.org/10.1242/jcs.049130

Deakin, N.O., C. Ballestrem, and C.E. Turner. 2012. Paxillin and Hic-5 interaction with vinculin is differentially regulated by Rac1 and RhoA. *PLoS ONE*. 7:e37990. http://dx.doi.org/10.1371/journal.pone.0037990

de Forges, H., A. Bouissou, and F. Perez. 2012. Interplay between microtubule dynamics and intracellular organization. *Int. J. Biochem. Cell Biol.* 44:266–274. http://dx.doi.org/10.1016/j.biocel.2011.11.009

Dowdy, S.C., S. Jiang, X.C. Zhou, X. Hou, F. Jin, K.C. Podratz, and S.W. Jiang. 2006. Histone deacetylase inhibitors and paclitaxel cause synergistic effects on apoptosis and microtubule stabilization in papillary serous endometrial cancer cells. *Mol. Cancer Ther.* 5:2767–2776. http://dx.doi.org/10.1158/1535-7163.MCT-06-0209

Doyle, A.D., F.W. Wang, K. Matsumoto, and K.M. Yamada. 2009. One-dimensional topography underlies three-dimensional fibrillar cell migration. *J. Cell Biol.* 184:481–490. http://dx.doi.org/10.1083/jcb.200810041

Efimov, A., N. Schiefermeier, I. Grigoriev, R. Ohi, M.C. Brown, C.E. Turner, J.V. Small, and I. Kaverina. 2008. Paxillin-dependent stimulation of microtubule catastrophes at focal adhesion sites. *J. Cell Sci.* 121:196–204. http://dx.doi.org/10.1242/jcs.012666

Ezratty, E.J., M.A. Partridge, and G.G. Gundersen. 2005. Microtubule-induced focal adhesion disassembly is mediated by dynamin and focal adhesion kinase. *Nat. Cell Biol.* 7:581–590. http://dx.doi.org/10.1038/ncb1262

Gupta, G.P., and J. Massagué. 2006. Cancer metastasis: building a framework. *Cell*. 127:679–695. http://dx.doi.org/10.1016/j.cell.2006.11.001

Hagel, M., E.L. George, A. Kim, R. Tamimi, S.L. Opitz, C.E. Turner, A. Imamoto, and S.M. Thomas. 2002. The adaptor protein paxillin is essential for normal development in the mouse and is a critical transducer of fibronectin signaling. *Mol. Cell. Biol.* 22:901–915. http://dx.doi.org/10.1128/MCB.22.3.901-915.2002

Haggarty, S.J., K.M. Koeller, J.C. Wong, C.M. Grozinger, and S.L. Schreiber. 2003. Domain-selective small-molecule inhibitor of histone deacetylase 6 (HDAC6)-mediated tubulin deacetylation. *Proc. Natl. Acad. Sci. USA*. 100:4389–4394. http://dx.doi.org/10.1073/pnas.0430973100

Houliston, E., and B. Maro. 1989. Posttranslational modification of distinct microtubule subpopulations during cell polarization and differentiation in the mouse preimplantation embryo. *J. Cell Biol.* 108:543–551. http://dx.doi.org/10.1083/jcb.108.2.543

Hubbert, C., A. Guardiola, R. Shao, Y. Kawaguchi, A. Ito, A. Nixon, M. Yoshida, X.F. Wang, and T.P. Yao. 2002. HDAC6 is a microtubule-associated deacetylase. *Nature*. 417:455–458. http://dx.doi.org/10.1038/417455a

Hurd, D.D., and W.M. Saxton. 1996. Kinesin mutations cause motor neuron disease phenotypes by disrupting fast axonal transport in *Drosophila*. *Genetics*. 144:1075–1085.

Inoue, H., K. Shiraki, S. Ohmori, T. Sakai, M. Deguchi, T. Yamanaka, H. Okano, and T. Nakano. 2002. Histone deacetylase inhibitors sensitize human colonic adenocarcinoma cell lines to TNF-related apoptosis inducing ligand-mediated apoptosis. *Int. J. Mol. Med.* 9:521–525.

Kaluza, D., J. Kroll, S. Gesierich, T.P. Yao, R.A. Boon, E. Hergenreider, M. Tjwa, L. Rössig, E. Seto, H.G. Augustin, et al. 2011. Class IIb HDAC6 regulates endothelial cell migration and angiogenesis by deacetylation of cortactin. *EMBO J.* 30:4142–4156. http://dx.doi.org/10.1038/emboj.2011.298

Kanno, K., S. Kanno, H. Nitta, N. Uesugi, T. Sugai, T. Masuda, G. Wakabayashi, and C. Maesawa. 2012. Overexpression of histone deacetylase 6 contributes to accelerated migration and invasion activity of hepatocellular carcinoma cells. *Oncol. Rep.* 28:867–873.

Kaverina, I., O. Krylyshkina, and J.V. Small. 1999. Microtubule targeting of substrate contacts promotes their relaxation and dissociation. *J. Cell Biol.* 146:1033–1044. http://dx.doi.org/10.1083/jcb.146.5.1033

Kaverina, I., O. Krylyshkina, and J.V. Small. 2002. Regulation of substrate adhesion dynamics during cell motility. *Int. J. Biochem. Cell Biol.* 34:746–761. http://dx.doi.org/10.1016/S1357-2725(01)00171-6

Kawaguchi, Y., J.J. Kovacs, A. McLaurin, J.M. Vance, A. Ito, and T.P. Yao. 2003. The deacetylase HDAC6 regulates aggresome formation and cell viability in response to misfolded protein stress. *Cell*. 115:727–738. http://dx.doi.org/10.1016/S0092-8674(03)00939-5

Kovacs, J.J., P.J. Murphy, S. Gaillard, X. Zhao, J.T. Wu, C.V. Nicchitta, M. Yoshida, D.O. Toft, W.B. Pratt, and T.P. Yao. 2005. HDAC6 regulates Hsp90 acetylation and chaperone-dependent activation of glucocorticoid receptor. *Mol. Cell*. 18:601–607. http://dx.doi.org/10.1016/j.molcel.2005.04.021

Krylyshkina, O., I. Kaverina, W. Kranewitter, W. Steffen, M.C. Alonso, R.A. Cross, and J.V. Small. 2002. Modulation of substrate adhesion dynamics via microtubule targeting requires kinesin-1. *J. Cell Biol.* 156:349–359. http://dx.doi.org/10.1083/jcb.200105051

Lafarga, V., I. Aymerich, O. Tapia, F. Mayor Jr., and P. Penela. 2012. A novel GRK2/HDAC6 interaction modulates cell spreading and motility. *EMBO J.* 31:856–869. http://dx.doi.org/10.1038/emboj.2011.466

League, G.P., and S.C. Nam. 2011. Role of kinesin heavy chain in Crumbs localization along the rhabdomere elongation in *Drosophila* photoreceptor. *PLoS ONE*. 6:e21218. http://dx.doi.org/10.1371/journal.pone.0021218

Lee, Y.S., K.H. Lim, X. Guo, Y. Kawaguchi, Y. Gao, T. Barrientos, P. Ordentlich, X.F. Wang, C.M. Counter, and T.P. Yao. 2008. The cytoplasmic deacetylase HDAC6 is required for efficient oncogenic tumorigenesis. *Cancer Res.* 68:7561–7569. http://dx.doi.org/10.1158/0008-5472.CAN-08-0188

Li, B., A. Samanta, X. Song, K.T. Iacono, K. Bembas, R. Tao, S. Basu, J.L. Riley, W.W. Hancock, Y. Shen, et al. 2007. FOXP3 interactions with histone acetyltransferase and class II histone deacetylases are required for repression. *Proc. Natl. Acad. Sci. USA*. 104:4571–4576. http://dx.doi.org/10.1073/pnas.0700298104

Li, L., D. Wei, Q. Wang, J. Pan, R. Liu, X. Zhang, and L. Bao. 2012. MEC-17 deficiency leads to reduced α-tubulin acetylation and impaired migration of cortical neurons. *J. Neurosci.* 32:12673–12683. http://dx.doi.org/10.1523/JNEUROSCI.0016-12.2012

Ling, S.C., P.S. Fahrner, W.T. Greenough, and V.I. Gelfand. 2004. Transport of *Drosophila* fragile X mental retardation protein-containing ribonucleoprotein granules by kinesin-1 and cytoplasmic dynein. *Proc. Natl. Acad. Sci. USA*. 101:17428–17433. http://dx.doi.org/10.1073/pnas.0408114101

Lippincott-Schwartz, J., N.B. Cole, A. Marotta, P.A. Conrad, and G.S. Bloom. 1995. Kinesin is the motor for microtubule-mediated Golgi-to-ER membrane traffic. *J. Cell Biol.* 128:293–306. (published errata appear in *J. Cell Biol.* 1995. 128:991 and *J. Cell Biol.* 1995. 129:893) http://dx.doi.org/10.1083/jcb.128.3.293

Liu, Y., L. Peng, E. Seto, S. Huang, and Y. Qiu. 2012. Modulation of histone deacetylase 6 (HDAC6) nuclear import and tubulin deacetylase activity through acetylation. *J. Biol. Chem.* 287:29168–29174. http://dx.doi.org/10.1074/jbc.M112.371120

Maruta, H., K. Greer, and J.L. Rosenbaum. 1986. The acetylation of α-tubulin and its relationship to the assembly and disassembly of microtubules. *J. Cell Biol.* 103:571–579. http://dx.doi.org/10.1083/jcb.103.2.571

Matov, A., K. Applegate, P. Kumar, C. Thoma, W. Krek, G. Danuser, and T. Wittmann. 2010. Analysis of microtubule dynamic instability using a plus-end growth marker. *Nat. Methods*. 7:761–768. http://dx.doi.org/10.1038/nmeth.1493

Matsuyama, A., T. Shimazu, Y. Sumida, A. Saito, Y. Yoshimatsu, D. Seigneurin-Berny, H. Osada, Y. Komatsu, N. Nishino, S. Khochbin, et al. 2002. In vivo destabilization of dynamic microtubules by HDAC6-mediated deacetylation. *EMBO J.* 21:6820–6831. http://dx.doi.org/10.1093/emboj/cdf682

Miller, P.M., A.W. Folkmann, A.R. Maia, N. Efimova, A. Efimov, and I. Kaverina. 2009. Golgi-derived CLASP-dependent microtubules control Golgi organization and polarized trafficking in motile cells. *Nat. Cell Biol.* 11:1069–1080. http://dx.doi.org/10.1038/ncb1920

Montagnac, G., V. Meas-Yedid, M. Irondelle, A. Castro-Castro, M. Franco, T. Shida, M.V. Nachury, A. Benmerah, J.C. Olivo-Marin, and P. Chavrier. 2013. αTAT1 catalyses microtubule acetylation at clathrin-coated pits. *Nature*. 502:567–570. http://dx.doi.org/10.1038/nature12571

Nagasaki, T., and G.G. Gundersen. 1996. Depletion of lysophosphatidic acid triggers a loss of oriented detyrosinated microtubules in motile fibroblasts. *J. Cell Sci.* 109:2461–2469.

North, B.J., B.L. Marshall, M.T. Borra, J.M. Denu, and E. Verdin. 2003. The human Sir2 ortholog, SIRT2, is an NAD^+-dependent tubulin deacetylase. *Mol. Cell*. 11:437–444. http://dx.doi.org/10.1016/S1097-2765(03)00038-8

Osmani, N., F. Peglion, P. Chavrier, and S. Etienne-Manneville. 2010. Cdc42 localization and cell polarity depend on membrane traffic. *J. Cell Biol.* 191:1261–1269. http://dx.doi.org/10.1083/jcb.201003091

Palazzo, A.F., C.H. Eng, D.D. Schlaepfer, E.E. Marcantonio, and G.G. Gundersen. 2004. Localized stabilization of microtubules by integrin- and FAK-facilitated Rho signaling. *Science*. 303:836–839. http://dx.doi.org/10.1126/science.1091325

Pankov, R., Y. Endo, S. Even-Ram, M. Araki, K. Clark, E. Cukierman, K. Matsumoto, and K.M. Yamada. 2005. A Rac switch regulates random versus directionally persistent cell migration. *J. Cell Biol.* 170:793–802. http://dx.doi.org/10.1083/jcb.200503152

Piperno, G., M. LeDizet, and X.J. Chang. 1987. Microtubules containing acetylated α-tubulin in mammalian cells in culture. *J. Cell Biol.* 104:289–302. http://dx.doi.org/10.1083/jcb.104.2.289

Provenzano, P.P., K.W. Eliceiri, J.M. Campbell, D.R. Inman, J.G. White, and P.J. Keely. 2006. Collagen reorganization at the tumor-stromal interface facilitates local invasion. *BMC Med.* 4:38. http://dx.doi.org/10.1186/1741-7015-4-38

Pugacheva, E.N., S.A. Jablonski, T.R. Hartman, E.P. Henske, and E.A. Golemis. 2007. HEF1-dependent Aurora A activation induces disassembly of the primary cilium. *Cell*. 129:1351–1363. http://dx.doi.org/10.1016/j.cell.2007.04.035

Puthenveedu, M.A., C. Bachert, S. Puri, F. Lanni, and A.D. Linstedt. 2006. GM130 and GRASP65-dependent lateral cisternal fusion allows uniform Golgi-enzyme distribution. *Nat. Cell Biol.* 8:238–248. http://dx.doi.org/10.1038/ncb1366

Reed, N.A., D. Cai, T.L. Blasius, G.T. Jih, E. Meyhofer, J. Gaertig, and K.J. Verhey. 2006. Microtubule acetylation promotes kinesin-1 binding and transport. *Curr. Biol.* 16:2166–2172. http://dx.doi.org/10.1016/j.cub.2006.09.014

Rey, M., M. Irondelle, F. Waharte, F. Lizarraga, and P. Chavrier. 2011. HDAC6 is required for invadopodia activity and invasion by breast tumor cells. *Eur. J. Cell Biol.* 90:128–135. http://dx.doi.org/10.1016/j.ejcb.2010.09.004

Ridley, A.J., M.A. Schwartz, K. Burridge, R.A. Firtel, M.H. Ginsberg, G. Borisy, J.T. Parsons, and A.R. Horwitz. 2003. Cell migration: integrating signals from front to back. *Science*. 302:1704–1709. http://dx.doi.org/10.1126/science.1092053

Rodionov, V.I., F.K. Gyoeva, E. Tanaka, A.D. Bershadsky, J.M. Vasiliev, and V.I. Gelfand. 1993. Microtubule-dependent control of cell shape and pseudopodial activity is inhibited by the antibody to kinesin motor domain. *J. Cell Biol.* 123:1811–1820. http://dx.doi.org/10.1083/jcb.123.6.1811

Ryan, S.D., K. Bhanot, A. Ferrier, Y. De Repentigny, A. Chu, A. Blais, and R. Kothary. 2012. Microtubule stability, Golgi organization, and transport flux require dystonin-a2–MAP1B interaction. *J. Cell Biol.* 196:727–742. http://dx.doi.org/10.1083/jcb.201107096

Sakuma, T., K. Uzawa, T. Onda, M. Shiiba, H. Yokoe, T. Shibahara, and H. Tanzawa. 2006. Aberrant expression of histone deacetylase 6 in oral squamous cell carcinoma. *Int. J. Oncol.* 29:117–124.

Schatten, G., C. Simerly, D.J. Asai, E. Szöke, P. Cooke, and H. Schatten. 1988. Acetylated alpha-tubulin in microtubules during mouse fertilization and early development. *Dev. Biol.* 130:74–86. http://dx.doi.org/10.1016/0012-1606(88)90415-0

Schmoranzer, J., G. Kreitzer, and S.M. Simon. 2003. Migrating fibroblasts perform polarized, microtubule-dependent exocytosis towards the leading edge. *J. Cell Sci.* 116:4513–4519. http://dx.doi.org/10.1242/jcs.00748

Skoufias, D.A., T.L. Burgess, and L. Wilson. 1990. Spatial and temporal colocalization of the Golgi apparatus and microtubules rich in detyrosinated tubulin. *J. Cell Biol.* 111:1929–1937. http://dx.doi.org/10.1083/jcb.111.5.1929

Steeg, P.S. 2006. Tumor metastasis: mechanistic insights and clinical challenges. *Nat. Med.* 12:895–904. http://dx.doi.org/10.1038/nm1469

Stehbens, S., and T. Wittmann. 2012. Targeting and transport: How microtubules control focal adhesion dynamics. *J. Cell Biol.* 198:481–489. http://dx.doi.org/10.1083/jcb.201206050

Theisen, U., E. Straube, and A. Straube. 2012. Directional persistence of migrating cells requires Kif1C-mediated stabilization of trailing adhesions. *Dev. Cell*. 23:1153–1166. http://dx.doi.org/10.1016/j.devcel.2012.11.005

Thyberg, J., and S. Moskalewski. 1993. Relationship between the Golgi complex and microtubules enriched in detyrosinated or acetylated alpha-tubulin: studies on cells recovering from nocodazole and cells in the terminal phase of cytokinesis. *Cell Tissue Res.* 273:457–466. http://dx.doi.org/10.1007/BF00333700

Thyberg, J., and S. Moskalewski. 1999. Role of microtubules in the organization of the Golgi complex. *Exp. Cell Res.* 246:263–279. http://dx.doi.org/10.1006/excr.1998.4326

Tran, A.D., T.P. Marmo, A.A. Salam, S. Che, E. Finkelstein, R. Kabarriti, H.S. Xenias, R. Mazitschek, C. Hubbert, Y. Kawaguchi, et al. 2007. HDAC6 deacetylation of tubulin modulates dynamics of cellular adhesions. *J. Cell Sci.* 120:1469–1479. http://dx.doi.org/10.1242/jcs.03431

Valenzuela-Fernández, A., S. Alvarez, M. Gordon-Alonso, M. Barrero, A. Ursa, J.R. Cabrero, G. Fernández, S. Naranjo-Suárez, M. Yáñez-Mo, J.M. Serrador, et al. 2005. Histone deacetylase 6 regulates human immunodeficiency virus type 1 infection. *Mol. Biol. Cell*. 16:5445–5454. http://dx.doi.org/10.1091/mbc.E05-04-0354

Valenzuela-Fernández, A., J.R. Cabrero, J.M. Serrador, and F. Sánchez-Madrid. 2008. HDAC6: a key regulator of cytoskeleton, cell migration and cell-cell interactions. *Trends Cell Biol.* 18:291–297. http://dx.doi.org/10.1016/j.tcb.2008.04.003

Wang, Y.H., Z.Q. Yan, Y.X. Qi, B.B. Cheng, X.D. Wang, D. Zhao, B.R. Shen, and Z.L. Jiang. 2010. Normal shear stress and vascular smooth muscle cells modulate migration of endothelial cells through histone deacetylase 6 activation and tubulin acetylation. *Ann. Biomed. Eng.* 38:729–737. http://dx.doi.org/10.1007/s10439-009-9896-6

Webb, D.J., K. Donais, L.A. Whitmore, S.M. Thomas, C.E. Turner, J.T. Parsons, and A.F. Horwitz. 2004. FAK-Src signalling through paxillin, ERK and MLCK regulates adhesion disassembly. *Nat. Cell Biol.* 6:154–161. http://dx.doi.org/10.1038/ncb1094

Webster, D.R., and G.G. Borisy. 1989. Microtubules are acetylated in domains that turn over slowly. *J. Cell Sci.* 92:57–65.

Williams, K.A., M. Zhang, S. Xiang, C. Hu, J.Y. Wu, S. Zhang, M. Ryan, A.D. Cox, C.J. Der, B. Fang, et al. 2013. Extracellular signal-regulated kinase (ERK) phosphorylates histone deacetylase 6 (HDAC6) at serine 1035 to stimulate cell migration. *J. Biol. Chem.* 288:33156–33170. http://dx.doi.org/10.1074/jbc.M113.472506

Yadav, S., S. Puri, and A.D. Linstedt. 2009. A primary role for Golgi positioning in directed secretion, cell polarity, and wound healing. *Mol. Biol. Cell*. 20:1728–1736. http://dx.doi.org/10.1091/mbc.E08-10-1077

Yu, J.A., N.O. Deakin, and C.E. Turner. 2009. Paxillin-kinase-linker tyrosine phosphorylation regulates directional cell migration. *Mol. Biol. Cell*. 20:4706–4719. http://dx.doi.org/10.1091/mbc.E09-07-0548

Zaidel-Bar, R., S. Itzkovitz, A. Ma'ayan, R. Iyengar, and B. Geiger. 2007. Functional atlas of the integrin adhesome. *Nat. Cell Biol.* 9:858–867. http://dx.doi.org/10.1038/ncb0807-858

Zhang, X., Z. Yuan, Y. Zhang, S. Yong, A. Salas-Burgos, J. Koomen, N. Olashaw, J.T. Parsons, X.J. Yang, S.R. Dent, et al. 2007. HDAC6 modulates cell motility by altering the acetylation level of cortactin. *Mol. Cell*. 27:197–213. http://dx.doi.org/10.1016/j.molcel.2007.05.033

Zhang, Y., S. Kwon, T. Yamaguchi, F. Cubizolles, S. Rousseaux, M. Kneissel, C. Cao, N. Li, H.L. Cheng, K. Chua, et al. 2008. Mice lacking histone deacetylase 6 have hyperacetylated tubulin but are viable and develop normally. *Mol. Cell. Biol.* 28:1688–1701. http://dx.doi.org/10.1128/MCB.01154-06

Zhu, J., C.B. Coyne, and S.N. Sarkar. 2011. PKC alpha regulates Sendai virus-mediated interferon induction through HDAC6 and β-catenin. *EMBO J.* 30:4838–4849. http://dx.doi.org/10.1038/emboj.2011.351

Zuo, Q., W. Wu, X. Li, L. Zhao, and W. Chen. 2012. HDAC6 and SIRT2 promote bladder cancer cell migration and invasion by targeting cortactin. *Oncol. Rep.* 27:819–824.